

As a library, NLM provides access to scientific literature. Inclusion in an NLM database does not imply endorsement of, or agreement with, the contents by NLM or the National Institutes of Health.

Learn more: [PMC Disclaimer](#) | [PMC Copyright Notice](#)



J Exp Bot. 2016 Nov 5;67(22):6459–6472. doi: [10.1093/jxb/erw418](https://doi.org/10.1093/jxb/erw418)

Wortmannin-induced vacuole fusion enhances amyloplast dynamics in *Arabidopsis zigzag1* hypocotyls

Ashley Ann Alvarez ¹, Sang Won Han ¹, Masatsugu Toyota ^{2,3,4}, Carla Brillada ¹, Jiameng Zheng ¹, Simon Gilroy ³, Marcela Rojas-Pierce ^{1*},

[Author information](#) [Article notes](#) [Copyright and License information](#)

PMCID: PMC5181587 PMID: [27816929](https://pubmed.ncbi.nlm.nih.gov/27816929/)

Highlight

The highly restricted movement of amyloplasts in graviperceptive cells of *zig-1* hypocotyls is overcome by wortmannin treatment, suggesting a physical association between amyloplasts and the vacuole.

Key words: Amyloplasts, cytoskeleton, gravitropism, SNARE, vacuole, wortmannin.

Abstract

Gravitropism in *Arabidopsis* shoots depends on the sedimentation of amyloplasts in the endodermis, and a complex interplay between the vacuole and F-actin. Gravity response is inhibited in *zigzag-1* (*zig-1*), a mutant allele of *VT111*, which encodes a SNARE protein involved in vacuole fusion. *zig-1* seedlings have fragmented vacuoles that fuse after treatment with wortmannin, an inhibitor of phosphatidylinositol 3-kinase, and underscore a role of phosphoinositides in vacuole fusion. Using live-cell imaging with a vertical stage microscope, we determined that young endodermal cells

below the apical hook that are smaller than 70 μm in length are the graviperceptive cells in dark-grown hypocotyls. This result was confirmed by local wortmannin application to the top of *zig-1* hypocotyls, which enhanced shoot gravitropism in *zig-1* mutants. Live-cell imaging of *zig-1* hypocotyl endodermal cells indicated that amyloplasts are trapped between juxtaposed vacuoles and their movement is severely restricted. Wortmannin-induced fusion of vacuoles in *zig-1* seedlings increased the formation of transvacuolar strands, enhanced amyloplast sedimentation and partially suppressed the agravitropic phenotype of *zig-1* seedlings. Hypergravity conditions at 10 g were not sufficient to displace amyloplasts in *zig-1*, suggesting the existence of a physical tether between the vacuole and amyloplasts. Our results overall suggest that vacuole membrane remodeling may be involved in regulating the association of vacuoles and amyloplasts during graviperception.

Introduction

Plants have the capacity to sense and respond to the direction of gravity by precise modulation of growth patterns in roots and shoots ([Hashiguchi et al., 2013](#)). Gravitropism involves mechanisms of perception, signal transduction and auxin-directed differential growth. According to the starch-statolith hypothesis, sedimentation of amyloplasts in response to gravity stimuli is critical for gravity sensing ([Masson et al., 2002](#)). Gravity perception in Arabidopsis shoots depends on the ability to sense the position of starch-filled amyloplasts, called statoliths, within shoot endodermal cells, or statocytes ([Fukaki et al., 1998](#)). This is supported by evidence that (i) mutants lacking an endodermis display agravitropic shoots ([Fukaki et al., 1998](#)), (ii) starchless mutants or mutants that lack amyloplasts show reduced gravitropism ([Kiss et al., 1997](#); [Weise and Kiss, 1999](#); [Fujihira et al., 2000](#)), (iii) hypergravity restored gravitropic sensitivity in starch-deficient mutants ([Fitzelle and Kiss, 2001](#)), and (iv) there is significant movement (sedimentation) of amyloplasts following gravistimulation ([Saito et al., 2005](#); [Hashiguchi et al., 2014](#)). The sedimentation of amyloplasts in shoot statocytes is thought to trigger downstream signaling events, including changes in the transport of and response to auxin ([Rakusova et al., 2011](#)). The early events of signal transduction for gravitropism remain largely unknown, although several genes have been suggested to function in its early phases ([Blancaflor and Masson, 2003](#)).

The current model of gravity sensing implicates the plant vacuole in the shoot gravity response ([Morita et al., 2002](#); [Yano et al., 2003](#); [Hashiguchi et al., 2013](#)). Shoot endodermal cells contain a large central vacuole that occupies most of the cell volume, and its role in gravity sensing is well established. Mutants with vacuolar defects, including mutant alleles of *SHOOT GRAVITROPISM6 (SGR6)*, *VTI11/ZIGZAG-1 (ZIG-1)/SGR4*, *SYNTAXIN OF PLANTS22 (SYP22)*/*SGR3* and *KATAMARI2 (KAM2)* were identified from screens for agravitropic shoots in Arabidopsis ([Fukaki et al., 1996b](#); [Yamauchi et al., 1997](#); [Kato et al., 2002](#); [Morita et al., 2002](#); [Yano et al., 2003](#); [Saito et al., 2005](#); [Hashiguchi et al., 2014](#)). A common phenotype in these mutants was the abnormal localization of amyloplasts in relation to the vacuole or abnormal vacuole morphology. In the case of *zig-1* mutants, the movement of amyloplasts in the endodermis of the inflorescence stem was greatly reduced ([Yano et al., 2003](#)). Both VTI11 and SYP22 are SNARE (soluble N-ethylmaleimide-sensitive factor attachment protein receptor) proteins that have important roles in membrane fusion at the vacuole, including homotypic vacuole fusion ([Chen and Scheller, 2001](#); [Wickner, 2010](#); [Zheng et al., 2014b](#)). Two

mutant alleles of *VT111*, *zig-1* and *impaired traffic to tonoplast3* (*itt3*), have multiple vacuoles per cell (Zheng *et al.*, 2014a,b). Treatment of *itt3* and *zig-1* with wortmannin (Wm), an inhibitor of phosphatidylinositol 3-kinase (PI3-kinase), resulted in vacuole fusion, and enhanced hypocotyl gravitropism (Zheng *et al.*, 2014b). This result is consistent with fragmented vacuoles being responsible for the agravitropic phenotype of *zig-1*. Two other proteins associated with endomembranes were implicated in gravitropism. KAT2 is a membrane-associated protein (Tamura *et al.*, 2007), and SGR6 is a HEAT-domain containing protein involved in vacuole membrane remodeling (Hashiguchi *et al.*, 2014). The roles of KAT2 or SGR6 in gravitropism are still unknown.

A tight association between amyloplasts and the large central vacuole has been described in inflorescence endodermal cells. In resting cells, amyloplasts are found at the bottom of the cell, where they undergo saltatory movements and are almost completely surrounded by the vacuole membrane (Morita *et al.*, 2002; Yano *et al.*, 2003; Morita, 2010).

Amyloplast sedimentation that results from changes in the gravity vector occurs inside transvacuolar strands (TVSs), and the amyloplasts remain tightly associated with the vacuolar membrane during this time (Saito *et al.*, 2005; Moirta *et al.*, 2012). TVSs may allow movement of organelles, and their formation requires actin filaments (Gao *et al.*, 2005; Leitz *et al.*, 2009; Moirta *et al.*, 2012). It is unclear if the F-actin inside TVSs is required for amyloplast association with the vacuole, sedimentation, or mechanisms of gravity perception (Morita, 2010; Blancaflor, 2013), but F-actin cables have been shown to associate with sedimenting amyloplasts inside TVSs (Saito *et al.*, 2005). However, the tight association between vacuole and amyloplasts was not disrupted by lantrunculin-B in wild-type inflorescences (Saito *et al.*, 2005). Overall, the mechanisms by which amyloplasts are so closely attached to vacuolar membranes, including TVSs, and the role of this interaction for gravitropism have not been elucidated. Interestingly, *kat2* mutants, which are agravitropic in shoots, develop fewer transvacuolar strands in leaves and petioles (Tamura *et al.*, 2007), but it is not known if this is the case for shoot endodermal cells. Even though a clear role for the vacuole in gravity perception is well established, the molecular mechanisms for vacuolar control or perception of amyloplast sedimentation has not been identified.

In addition to the vacuole, important roles for actin filaments have been reported, but their role during shoot gravitropic perception remains unclear (Blancaflor, 2013). Actin depolymerizing drugs have been reported to enhance gravity response in hypocotyls (Yamamoto and Kiss, 2002; Yamamoto *et al.*, 2002), reduce amyloplast sedimentation in endodermal cells (Palmieri and Kiss, 2005) or have no effect in experiments with live cells (Saito *et al.*, 2005). An important role of the actin cytoskeleton was demonstrated by the identification of the *shoot gravitropism9* (*sgr9*) mutant, which shows reduced amyloplast sedimentation due to increased interactions between amyloplasts and F-actin (Nakamura *et al.*, 2011). *SGR9* encodes an E3 ligase that may disrupt the attachment of amyloplasts to F-actin during saltatory movements and as a result promote amyloplast sedimentation (Nakamura *et al.*, 2011). The difficulty of establishing a role of F-actin in gravity perception may be due to the complexity of interactions that it may have with a multitude of cellular components, including amyloplasts.

Here we used live-cell imaging on a vertical stage microscope to demonstrate the role of the large central vacuole in

shoot gravitropism in seedlings. Our results identified the upper hypocotyl endodermis as the gravisensing tissue and highlight a novel tight interaction between the vacuolar membrane and amyloplasts. The fragmented vacuoles in endodermal cells of *zig-1* hypocotyls restrict amyloplast movement, contributing to the agravitropic phenotype of this mutant. We show that application of Wm to *zig-1* enhances their gravitropic response, restores amyloplast sedimentation and enhances the formation of TVSs. Additionally, we show that the tight association between vacuoles and amyloplasts observed in *zig-1* hypocotyls involves neither F-actin nor microtubules.

Materials and methods

Plant material and growth conditions

The *zig-1* mutant line was previously described ([Kato et al., 2002](#)). The parental and *itt3* lines contain the green fluorescent protein (GFP)-TIP2;1 and the mCherry-HDEL markers ([Zheng et al., 2014b](#)), and marker lines expressing the fluorescent protein fusions VHA-a1:GFP ([Dettmer et al., 2006](#)), ABD2-GFP ([Wang et al., 2004](#)) and TUA6-GFP ([Ueda et al., 1999](#)) were described before. Seeds were surface sterilized and incubated at 4 °C in the dark for 2–5 d. Seeds were sown on Arabidopsis growth medium (AGM; 0.5× Murashige and Skoog medium, 4 g l⁻¹ GelRite, 1% (w/v) sucrose) and transferred to a 22 °C growth chamber with 16 h/8 h day/night photoperiod. For dark grown experiments, plants were incubated in light for 8 h to stimulate germination prior to growth in the dark.

Plasmid construction and plant transformations

The *pSCR::TIP1;1-GFP* construct was generated by amplifying a 2 kb fragment corresponding to the *SCARECROW* promoter (pSCR2.0) from pENTR 5'pSCR2.0 ([Levesque et al., 2006](#); [Sozzani et al., 2010](#)) using primers 5'-AAGCTTGCCAAA CAGATATTGCATTGGGCTATG-3' and 5'-CTCGAGTAGG AGATTGAAGGGTTGTT-3'. The pSCR2.0 PCR fragment was cloned into VAC-GK ([Nelson et al., 2007](#)) by restriction enzyme and ligation with *Hind*III and *Xho*I to generate *pSCR::TIP1;1-GFP*. The resulting plasmid was then transformed into *zig-1* or Col-0 WT by the floral dip method ([Clough and Bent, 1998](#)).

Chemical stocks and treatments

All chemical treatments used 4-d-old seedlings unless otherwise specified. Stock solutions of 3.3 mM wortmannin (Sigma-Aldrich), 200 µM latrunculin B (Lat-B; Sigma-Aldrich), and 2 mM oryzalin (Sigma-Aldrich) were made in 100% (v/v) dimethyl sulfoxide (DMSO) and diluted to working concentrations in liquid AGM as 1% (v/v) DMSO, 33 µM Wm, 2 µM Lat-B and 20 µM oryzalin. Vacuole fusion assays were carried out by incubating seedlings in either DMSO or Wm for 90 min to 2 h before rinsing in diH₂O and imaging.

Lugol solution was purchased from Sigma-Aldrich (62650). Staining was carried out by submerging Col-0 WT seedlings in solution for 20 min, while maintaining their growth orientation. Next, they were washed in diH₂O for 10 min before they were mounted on microscope slides.

Microscopy

Imaging in a vertical stage was carried out with a Leica DM5000 compound microscope equipped with a Leica DFC365 FX camera, and a Leica $\times 40/1.0$ NA water objective was used. The microscope was outfitted with a custom-made 90° InverterScope objective inverter (LSM Technologies) between the objective turret and the $\times 40$ objective and a custom-made vertical stage (LSM Technologies) that included a manual rotation stage (Thor Labs). Bright-field imaging was accomplished by placing an aspheric condenser lens (cat. no. ACL1210-A, Thor Labs) inside the rotation stage ~10 mm behind the sample, and an adaptor was made by 3-D printing to attach the end of a light guide to the back of the vertical stage. The adaptor included a slit to slide a blocking sheet or a green filter (see [Supplementary Fig. S1](#) at JXB online). All imaging was done with the green filter inside the slit. Etiolated seedlings were affixed to slides using a very fine layer of Hollister Medical Adhesive ([Behera and Kudla, 2013](#)). A 1.0 mm silicon isolator (cat. no. CWS-13R-1.0, Grace BioLabs) and a coverslip were used to create a chamber filled with water, and Immersol 518 F (Carl Zeiss) was used as the immersion oil for the water objective.

A Zeiss LSM 710 confocal microscope with a $\times 40$ water objective (1.1 NA) or $\times 20$ objective (0.8 NA) was used for confocal microscopy. The excitation/emission wavelengths during acquisition were 488 nm/492–557 nm for GFP, and 516 nm/582–670 nm for mCherry. TVSs were counted as previously described ([Han et al., 2015](#)). Briefly, hypocotyls were imaged in 600 μm thick optical sections using a $\times 20$ (0.8 NA) objective to capture the volume of entire cells. Vacuolar membrane folds were counted as TVSs if they were formed by a double membrane, even if they did not transverse the entire vacuole in the XY plane.

A centrifuge microscope was used for hypergravity experiments as previously described ([Toyota et al., 2013a,b](#)). Four-day-old etiolated seedlings were mounted in a chamber to fix the specimen on the centrifuge microscope before rotation; 10 g was applied after 10–20s of imaging and held continuously for 60s.

Quantification of organelle movement

Tracking amyloplast movement was performed with the MTrackJ plugin of ImageJ. Amyloplast movement was quantified capturing time-lapse images for 3 min at 10 s intervals, but only amyloplasts that could be traced throughout all frames were scored. Seedlings were 4 d old for all experiments. The x , y coordinates of each amyloplast were recorded from each image. Then, the change in position in the x (Δx) and y (Δy) axes were determined and plotted in a coordinate graph. A stationary reference point such as the corner of a cell was used to correct for stage drift.

Tracking of amyloplasts during hypergravity experiments was carried out with G-Track spot-tracking software (G-Angstrom, Japan) as described ([Toyota et al., 2013a](#)).

Gravitropism assay and hypocotyl curvature

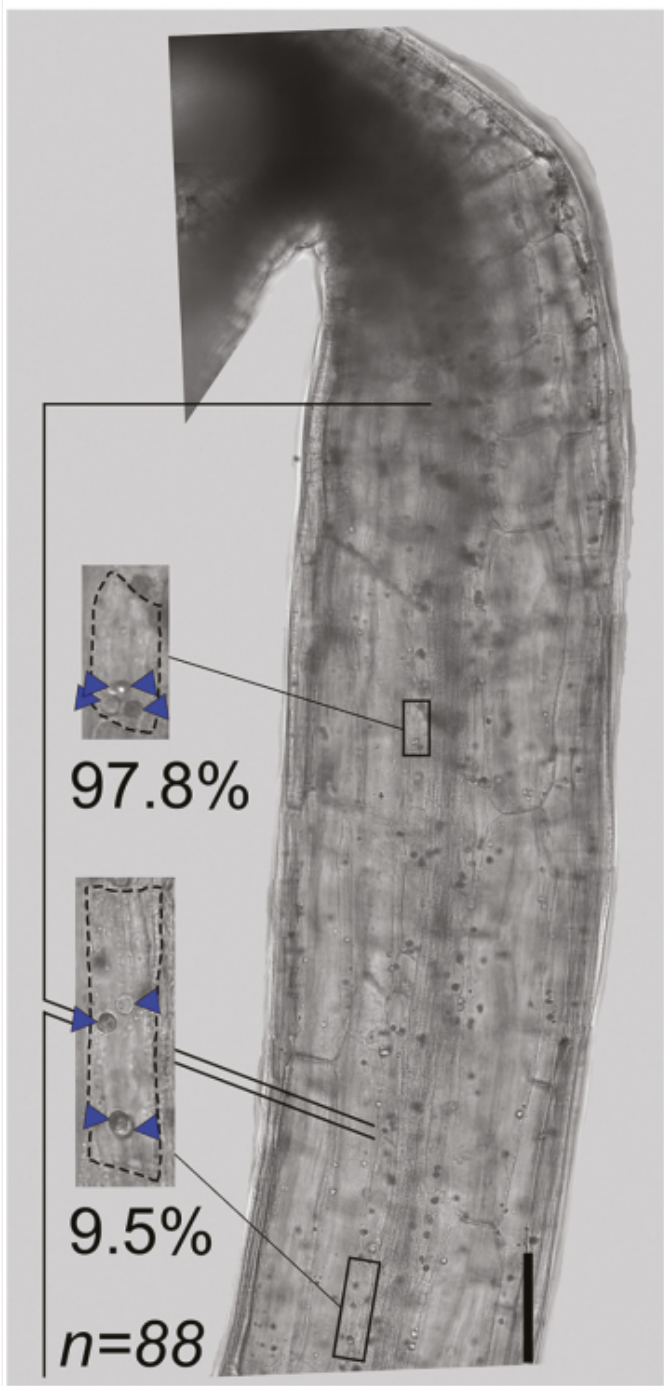
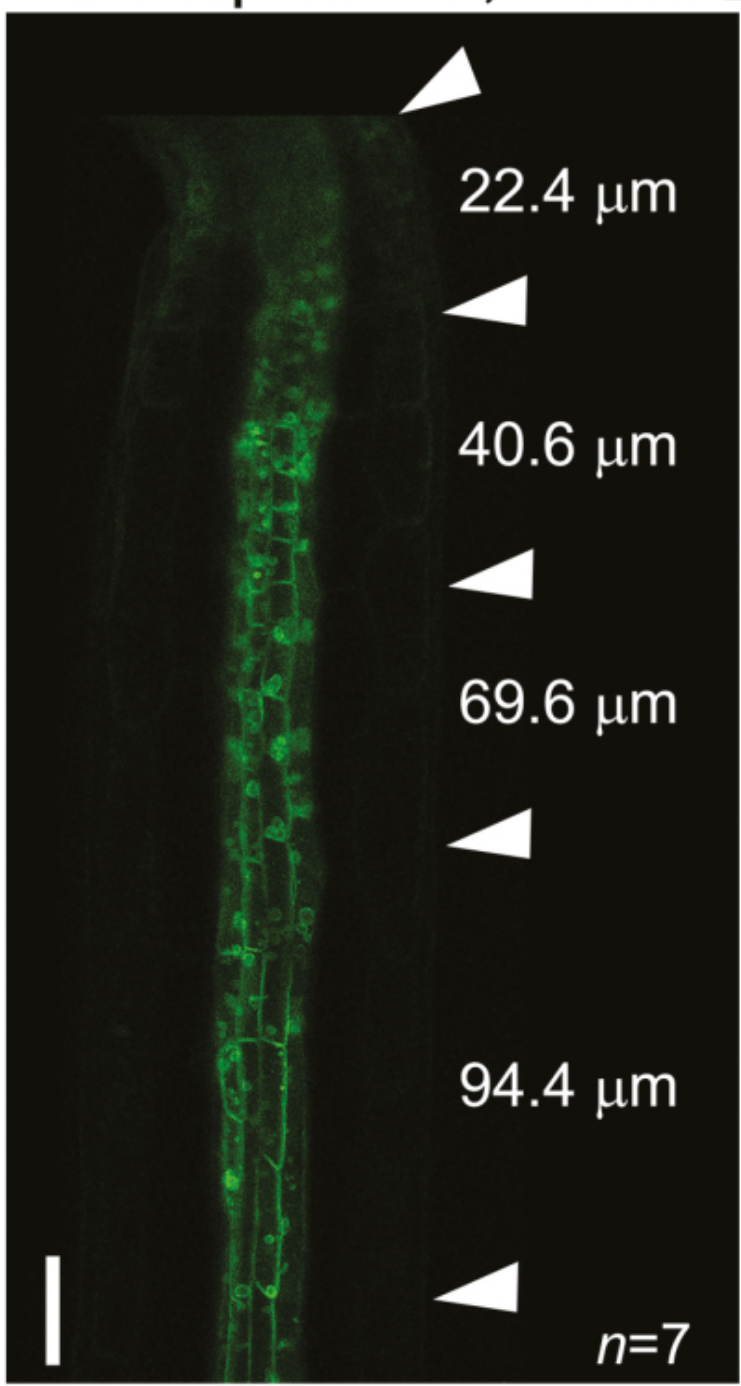
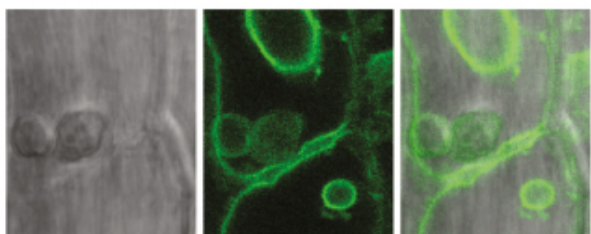
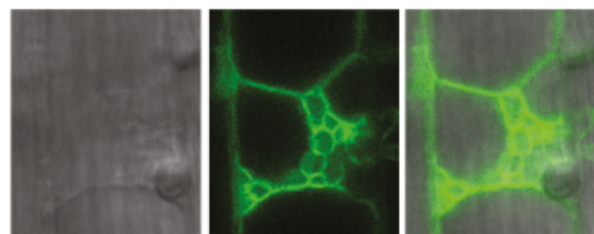
Col-0 WT and *zig-1* were sown on AGM, wrapped in foil to simulate dark, and oriented vertically for 3 d. All subsequent transfers took place in a dark room using a green safe light. Wm treatment was carried out by first aligning seedlings to the first gravity vector (*g*1) before placing an AGM dot containing either 1% (v/v) DMSO or 33 µM Wm on the top or bottom of the seedlings. For cytoskeleton inhibitor treatments, seedlings were transferred to fresh plates containing DMSO, 2 µM Lat-B or 20 µM oryzalin, and aligned to *g*1. Plates were wrapped in foil after transfers, rotated 90°, and scanned after another 20 h in the dark. ImageJ was used to measure hypocotyl curvature as the angle between the top of the hypocotyl and *g*1. All experiments were repeated at least three times.

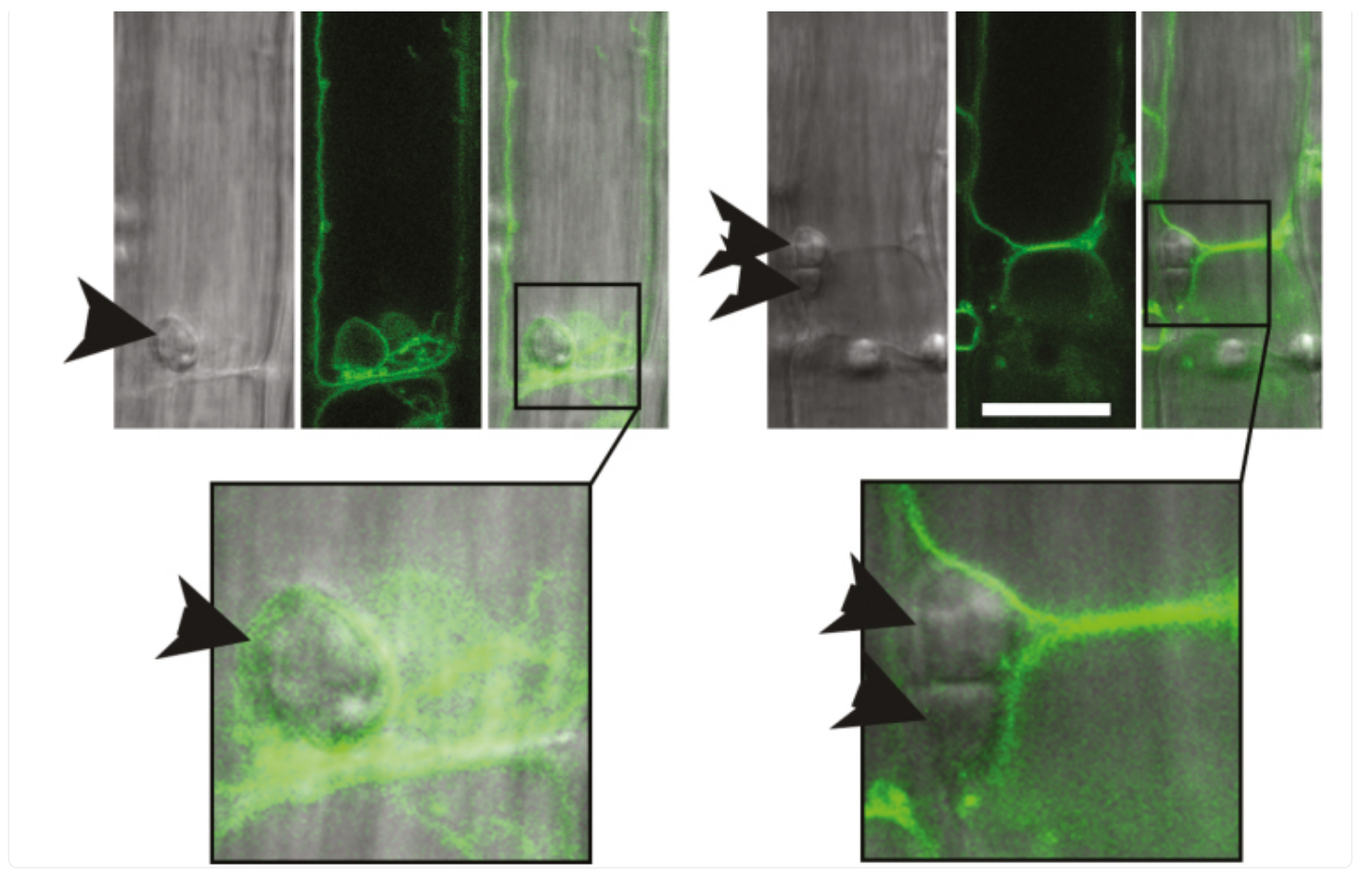
Results

Statocytes in etiolated hypocotyls are restricted to young cells below the apical hook

Amyloplast sedimentation in shoots has been well characterized by live-cell microscopy in inflorescence stems ([Morita et al., 2002](#); [Saito et al., 2005](#); [Toyota et al., 2013b](#)) but not in seedlings. In order to characterize mechanisms of gravity perception in seedlings, we first quantified amyloplast sedimentation in wild-type (WT) hypocotyl endodermal cells by Lugol staining ([Fig. 1A](#)). When cells from the upper portion of the hypocotyl were imaged, 97.8% of the amyloplasts were found sedimented in the direction of gravity. However, only 9.5% of amyloplasts were observed at the bottom of the cell when cells were imaged further down the hypocotyl. This result suggests that amyloplast sedimentation may be restricted to endodermal cells just below the apical hook.

Fig. 1.

A WT**B SCR_p::TIP1;1-GFP****C****SCR_p::TIP1;1-GFP****Col-0****zig-1**



[Open in new tab](#)

Graviperceptive cells are located just below the shoot apex. (A) Endodermal cells below the apical hook contain sedimented amyloplasts. Col-0 WT seedlings were stained with Lugol solution and imaged on a compound microscope while maintaining a vertical orientation. The insets show representative cells from the region just below the apical hook (top) or a region towards the middle of the hypocotyl (bottom). Percentages under the insets represent the proportion of amyloplasts found at the bottom of cells in each region of the hypocotyl. $n=88$ amyloplasts from 23 cells and three seedlings. Arrowheads indicate the position of amyloplasts. Scale bar: 100 μm . (B) Increase of cell length along the hypocotyl endodermis. Dark-grown Col-0 WT seedling expressing *pSCR::TIP1;1-GFP* were imaged by confocal microscopy. Average length of cells between the arrowhead marks is shown. Cell length data also include seedlings stained with Lugol solution and imaged by bright-field. $n=7$ seedlings. Scale bar: 100 μm . (C) Amyloplasts get trapped between vacuoles in *zig-1* endodermis. Endodermal cells near the shoot meristem of Col-0 WT (Col-0) and *zig-1* seedlings expressing *pSCR::TIP1;1-GFP* were imaged by bright-field and confocal microscopy. Arrowheads mark the position of amyloplasts. Insets show the association between tonoplast and amyloplast. Scale bar: 20 μm .

We measured cell length along the upper hypocotyl endodermis to better understand the potential transition between statocytes and non-statocytes. Cell length was estimated from bright-field images of Lugol-stained WT, as well as

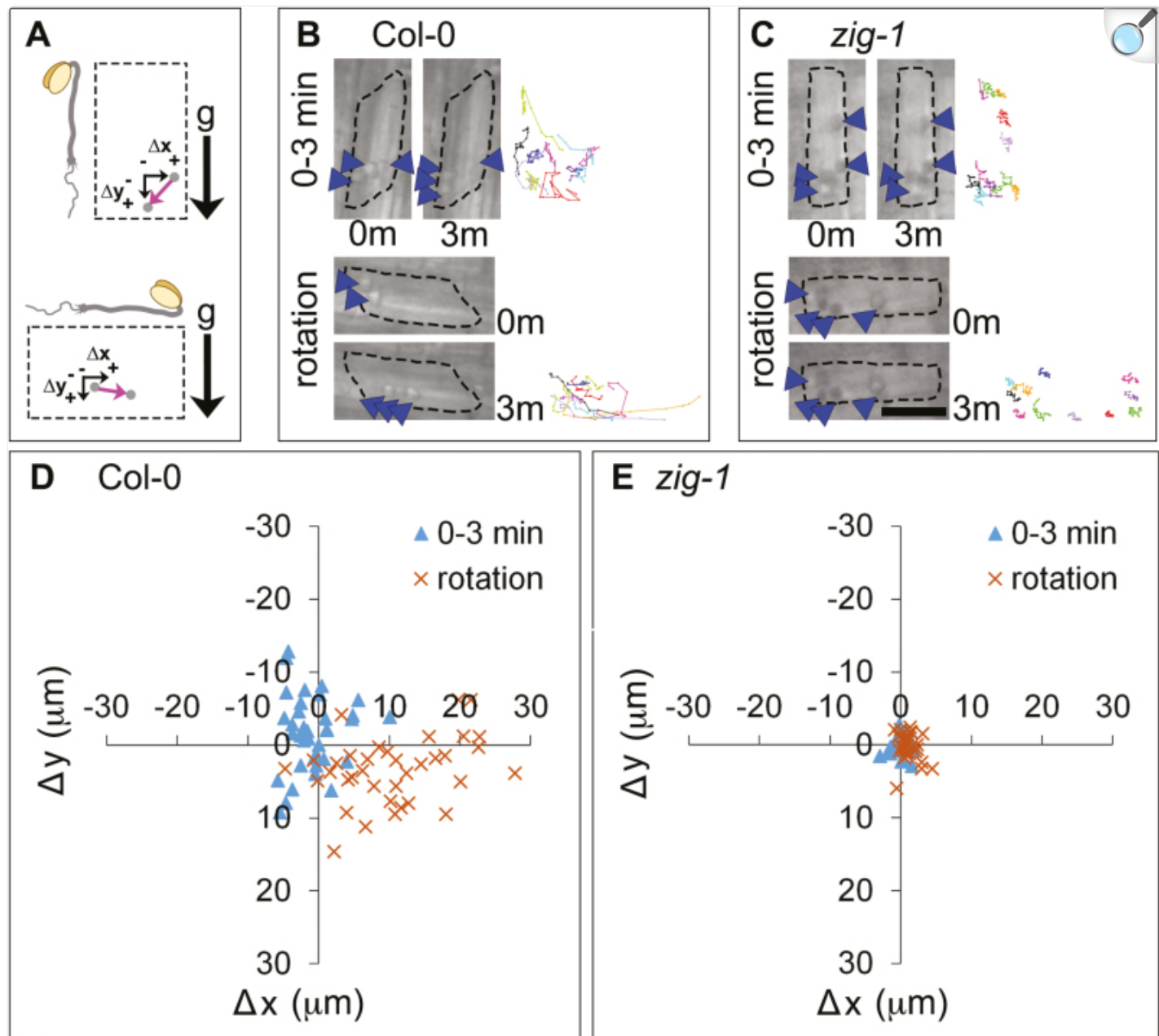
confocal images of a GFP-tagged vacuolar marker exclusively expressed in the endodermis (pSCR::TIP-1;1-GFP, Fig. 1B). Cell length varied from 23 ± 3.69 to 94 ± 0.82 μm in this region when measured from the apical hook to ~ 1 mm towards the root, but on average, only cells with length <70 μm showed sedimented amyloplasts. Using amyloplast sedimentation as a marker for the ability to perceive gravity, the small cells at the top of the hypocotyl are more likely to correspond to the shoot statocytes. Given this result, all subsequent experiments described below were conducted with endodermal cells between 30 and 70 μm in length within this region of the hypocotyl.

Amyloplasts in graviperceptive cells have been shown to be closely associated with the vacuole membrane (Morita *et al.*, 2002), and mutants in the SNARE protein VTI11 have abnormal vacuole morphology (Zheng *et al.*, 2014b) and agravitropic phenotypes (Kato *et al.*, 2002). The vacuole was visualized in WT and *zig-1* using the pSCR::TIP1;1-GFP marker in order to determine the relationship between the vacuole and amyloplast in seedlings. As expected, a large central vacuole occupies most of the volume of WT endodermal cells and the tonoplast surrounds the sedimented amyloplasts (Fig. 1C). In contrast, *zig-1* displays a fragmented vacuole phenotype in shoot endodermal cells, as previously described for other tissues (Zheng *et al.*, 2014b). It is important to note that amyloplasts do not sediment in *zig-1* mutants and appear to be trapped at the junction between two or more adjacent vacuoles (Fig. 1C). Furthermore, and similar to *zig-1* inflorescences (Morita *et al.*, 2002; Saito *et al.*, 2005), the tonoplast does not tightly surround the amyloplasts in *zig-1* hypocotyls. These results indicate that the vacuole phenotype of *zig-1* impinges on the distribution of amyloplasts in hypocotyl endodermal cells and likely prevents their sedimentation.

The dynamic behavior of endodermal amyloplasts is restricted in *zig-1*

A novel set-up for live-cell imaging on a vertical microscope was developed to identify mechanisms of vacuolar membrane dynamics involved in gravity perception or response (see Supplementary Fig. S1). Seedlings were grown vertically for 4 d before being mounted in a slide chamber and equilibrated for 5 min. Sequential images were acquired at 10 s intervals for 3 min (Saito *et al.*, 2005) in the vertical stage (Fig. 2A). Most WT amyloplasts were detected at the bottom of the cell between 0 and 3 min (Fig. 2B, 0–3 min), and organelle tracking indicates that they exhibited dynamic saltatory movements (Fig. 2B, 0–3 min). In contrast, *zig-1* amyloplasts were found more widely distributed in the cell between 0 and 3 min, and they were severely limited in their movement as shown by their comparatively static tracks (Fig. 2C). Next, seedlings were rotated 90° and imaged immediately for the following 3 min (Fig. 2A). Amyloplasts from WT sedimented in the direction of gravity after reorientation as shown by the organelle tracks between 0 and 3 min after rotation (Fig. 2B, rotation). In contrast, amyloplasts from *zig-1* continued to be much more limited in their movement even after a reorientation (Fig. 2C, rotation). These results, and those from inflorescences (Saito *et al.*, 2005), support the role of the central vacuole in shoot gravity sensing.

Fig. 2.



[Open in a new tab](#)

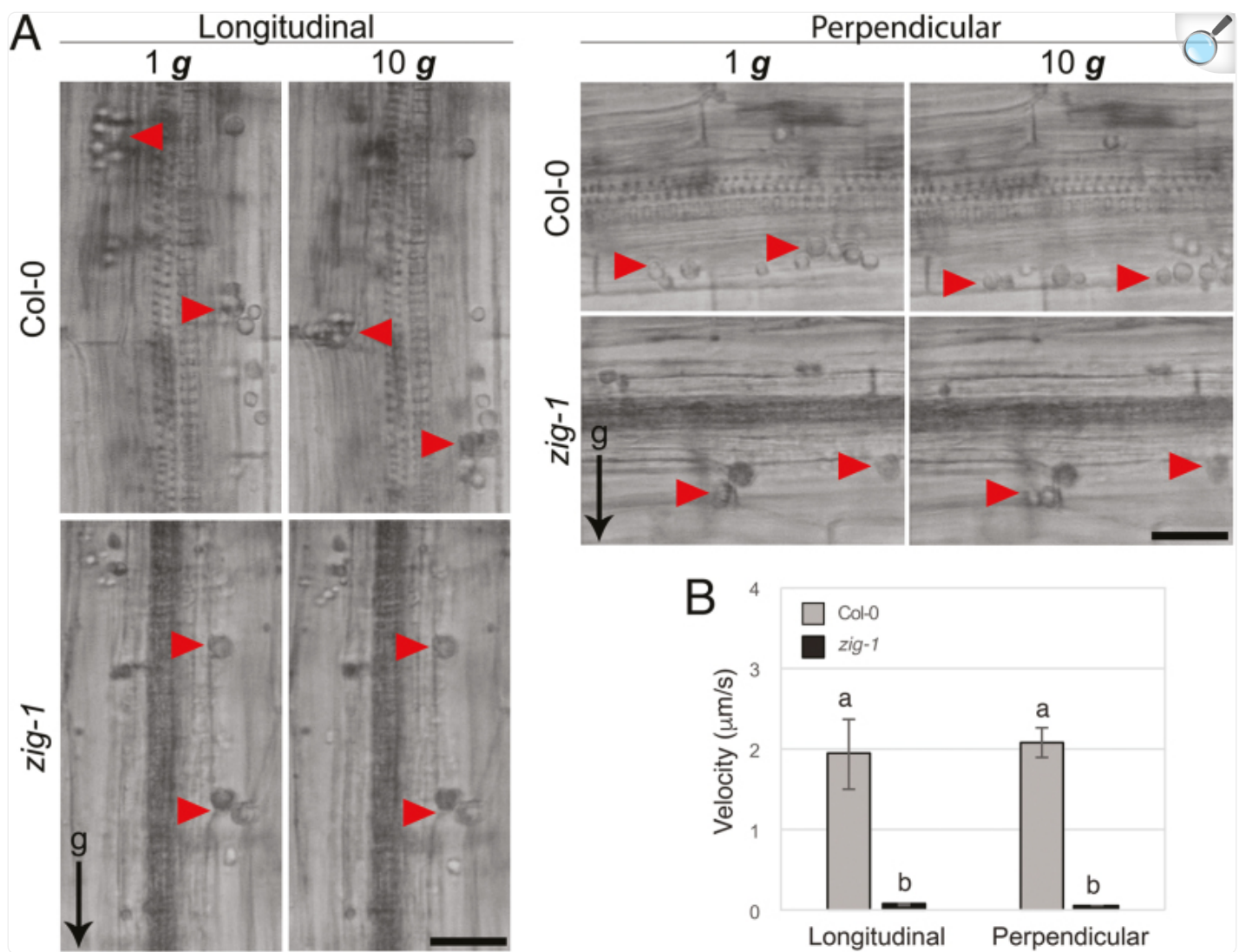
Amyloplast dynamics in hypocotyl endodermal cells before and after gravity reorientation. (A) Schematic representation of the rotation experiment. The orientation of the seedling with respect to gravity (g) before and after rotation is shown. Displacement of an amyloplast (gray circle) during a 3 min time lapse is shown with a pink arrow, and is expressed as a change in the horizontal position (Δx) and the vertical position (Δy). Positive values correspond to right and down and negative values correspond to left and up. (B, C) Amyloplast movements before and after rotation. A representative cell from the endodermis of *Col-0* WT (B)

or *zig-1* (C) is shown before (0–3 min) or after (rotation) a 90° rotation. Images correspond to the amyloplast positions at the start (0m) or the end (3m) of a 3 min time lapse. Tracks of representative amyloplasts are shown as different colored lines at the right of each panel. Arrowheads indicate one to two amyloplasts. Scale bar: 15 μm. (D, E) Quantification of amyloplast movements in WT and *zig-1* before and after rotation. Coordinate graph showing amyloplast displacement between 0 and 3 min in Col-0 WT (D) or *zig-1* (E). Time-lapse experiments were carried out either before (blue triangles) or after (orange crosses) a 90° rotation. $n=73$ amyloplasts from four seedlings of Col-0; $n=65$ amyloplasts from four seedlings of *zig-1*.

Quantification of amyloplast movement indicated that their movement in WT before rotation occurred in all directions for up to 10 μm ([Fig. 2D, E](#)). Following a 90° reorientation, most amyloplasts translocated to the new bottom of the cell (lower right quadrant of the graph) for up to 30 μm. On the other hand, amyloplast movement in *zig-1* was confined to <5 μm in all directions before reorientation, and there was little change in their position after a 90° reorientation ([Fig. 2E](#)). These results indicate that the fragmented vacuoles may impair movement of these organelles in *zig-1*.

Reduced amyloplast sedimentation in *zig-1* hypocotyls could be due to the physical impediments created by the fragmented vacuoles. To address this question, we utilized hypergravity conditions to increase sedimentary movement and analysed amyloplast behavior using a centrifuge microscope ([Toyota et al., 2013a,b](#)). Two types of gravistimulation were used at 10 g, one applied longitudinally (along the shoot–root longitudinal axis) and a second applied perpendicularly, similar to a 90° reorientation assay. Upon application of hypergravity in either direction, amyloplasts in WT moved and reached the edge of the cell within 60 s ([Fig. 3A](#)). Surprisingly, when 10 g was applied in either direction in *zig-1*, amyloplast movements were highly restricted ([Fig. 3A](#)), indicating a potential tight association between amyloplasts and the tonoplast itself. Measurements of amyloplast velocity indicated that these differences are significant ([Fig. 3B](#)). Collectively, these results suggest that failure of amyloplasts to sediment in *zig-1* is due to the abnormal vacuoles and a potential physical interaction between vacuoles and amyloplasts.

Fig. 3.



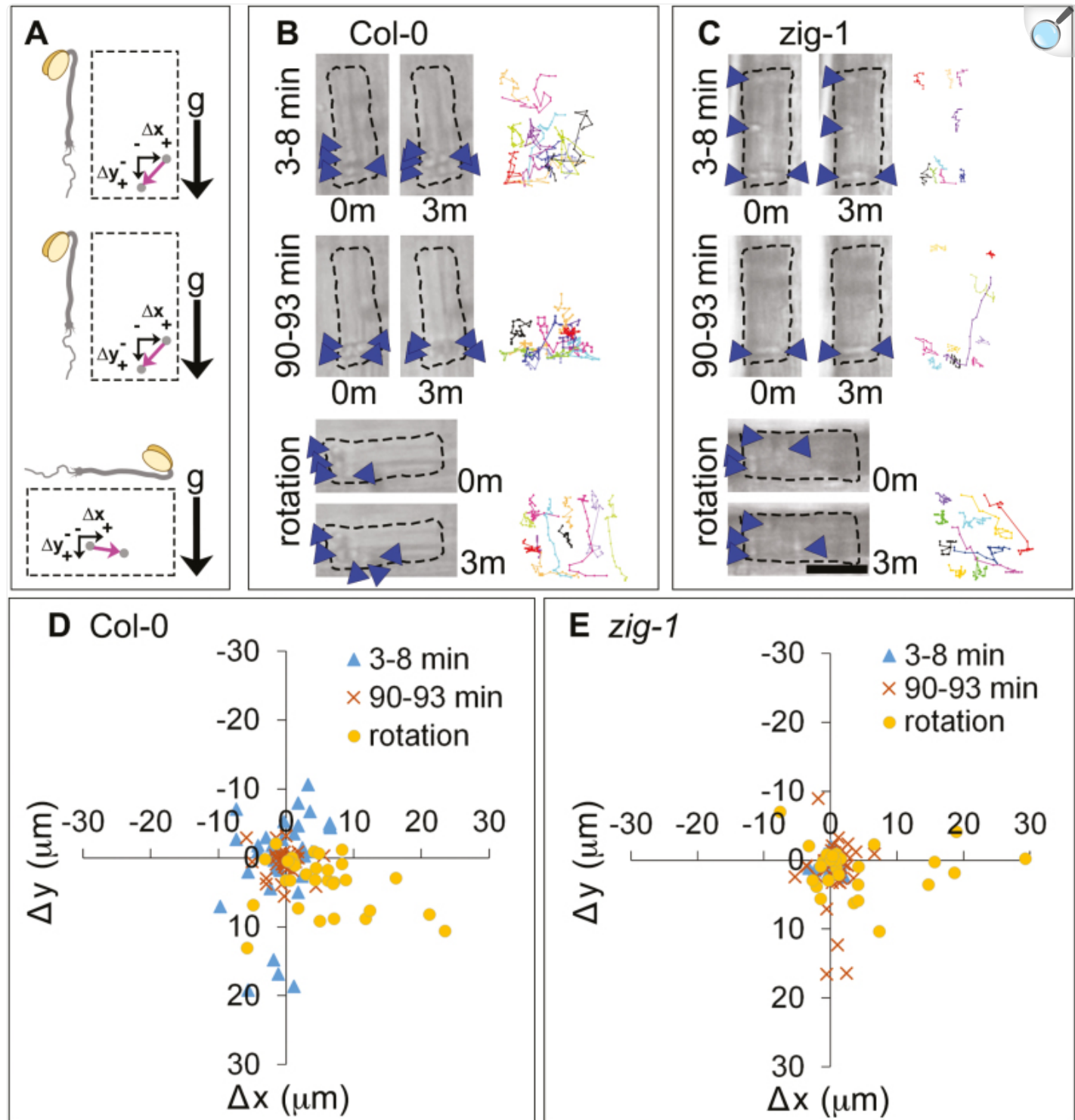
[Open in a new tab](#)

Hypergravity does not displace amyloplasts in the *zig-1* mutant. (A) Hypergravity (10 g) was applied either longitudinally or perpendicularly to 4-d-old dark grown WT and *zig-1* seedlings. Amyloplast localization was imaged by bright-field. Amyloplasts in WT relocate to the gravity associated bottom of the cell within 1 min of hypergravity; however, amyloplast movement in *zig-1* is much more restricted. Scale bar: 20 μ m. (B) The velocity of amyloplast movement in Col-0 and *zig-1* was analysed under the 10 g conditions. Data are shown as means and error bars represent standard error. Different letters denote significant differences among all four data ($P<0.05$, one-way ANOVA followed by the Tukey's multiple comparison test). $n=9\text{--}17$ amyloplasts. (This figure is available in color at *JXB* online.)

Wortmannin-induced vacuolar membrane fusion releases endodermal amyloplasts in *zig-1*

Wm was used to test the effect of vacuole fusion on amyloplast sedimentation. Wm inhibits PI3-kinase, reduces the amount of phosphatidylinositol 3-phosphate in cellular membranes ([Jung et al., 2002](#)), and induces vacuole fusion in *zig-1* ([Zheng et al., 2014b](#)). Seedlings were treated with 33 µM Wm in the vertical microscope stage (see [Supplementary Fig. S1](#) at JXB online), and time lapses were collected within 3–8 min of Wm application and after 90 min. [Figure 4A](#) shows the orientation of the seedlings throughout the experiment. No obvious differences in amyloplast dynamics were observed in WT seedlings 3–8 min after Wm application ([Fig. 4B](#), 3–8 min) when compared with the untreated control ([Fig. 2B](#)). Additionally, amyloplast movements still appeared severely limited in *zig-1* when seedlings were imaged within 8 min of Wm treatment ([Fig. 4C](#), 3–8 min). After 90 min of Wm treatment, WT amyloplasts were still sedimented in the direction of gravity, but the amplitude of saltatory movements seemed reduced ([Fig. 4B](#), 90–93 min). In contrast, 90 min of Wm treatment in *zig-1* resulted in many amyloplasts being found at the bottom of the cell ([Fig. 4C](#), 90–93 min), compared with the untreated *zig-1* ([Fig. 2C](#)). Seedlings were then rotated 90° and they were again imaged for 3 min immediately after. Upon reorientation, WT amyloplasts sedimented to the new gravity-associated cell bottom within 3 min ([Fig. 4B](#), rotation). Finally, several amyloplasts in Wm-treated *zig-1* sedimented in the direction of gravity following reorientation and their tracks were more similar to WT ([Fig. 4C](#), rotation). Collectively, these results suggest that Wm treatment, which induces vacuole fusion, is sufficient to release amyloplasts in the endodermis of *zig-1* hypocotyls.

Fig. 4.



[Open in a new tab](#)

Wortmannin treatment enhances amyloplast dynamics in *zig-1* hypocotyls. (A) Representation of the rotation experiment showing the orientation of the seedling with respect to gravity throughout the experiment.

Displacement of an amyloplast (grey circle) during a 3 min time lapse is shown with a pink arrow, and is expressed as a change in the horizontal (Δx) and the vertical (Δy) position. Positive values correspond to displacement to the right and down while negative values correspond to displacement towards the left and up. Seedlings were incubated vertically in the presence of 33 μM Wm and imaged immediately for 3 min (top, 3–8 min). Another 3 min time lapse was captured after 90 min of Wm treatment (middle, 90–93 min), and finally, seedlings were rotated 90° and a 3 min time lapse was captured immediately (bottom, rotation). (B, C) Amyloplast movements after a Wm treatment. A representative cell from the endodermis of Col-0 WT (B) or *zig-1* (C) was imaged immediately after Wm treatment (3–8 min), 90 min after Wm treatment (90–93 min) or 90 min after Wm treatment and a 90° rotation (rotation). Images correspond to the amyloplast positions at the start (0m) or the end (3m) of a 3 min time lapse. Tracks of representative amyloplasts are shown as different colored lines at the right of each panel. Arrowheads indicate one to two amyloplasts. Scale bar: 15 μm . (D, E) Quantification of amyloplast movements in WT and *zig-1* after Wm treatment. Coordinate graph showing amyloplast displacement between 0 and 3 min of each time lapse in Col-0 WT (D) or *zig-1* (E). Time lapse experiments were carried out within 3–8 min of Wm treatment (blue triangle), after 90 min of Wm treatment before rotation (orange crosses), or after 93 min of Wm treatment followed by a 90° rotation (yellow circles). $n=110$ amyloplasts from four seedlings of Col-0; $n=98$ amyloplasts from four seedlings of *zig-1*.

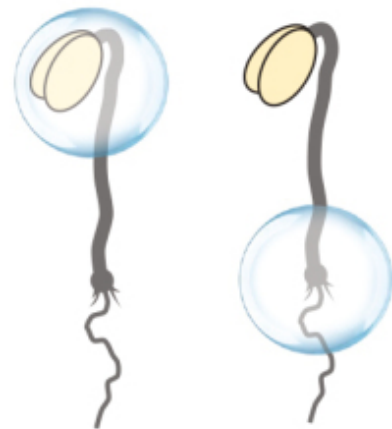
Quantification of amyloplast movements during these experiments indicated that amyloplast saltatory motion in WT was large (up to 20 μm) and showed no obvious bias in direction shortly after Wm treatment (Fig. 4D, 3–8 min). However, Wm treatment for 90 min restricted amyloplast movement in WT to within 10 μm of their initial position (Fig. 4D, 90–93 min). Again, most amyloplasts were able to translocate to the new gravity-associated bottom of the cell following the reorientation (Fig. 4D, rotation). In contrast, Wm treatment of *zig-1* mutants had dramatic effects on amyloplast movement. Initially, *zig-1* amyloplast movement was highly restricted to within 5 μm of their starting position immediately after Wm application (Fig. 4E, 3–8 min) in a similar fashion to untreated seedlings (Fig. 2C). However, after 90 min their range of motion had increased to within 10 μm , and sometimes up to 17 μm from their original position (Fig. 4E, 90–93 min). After rotation, several amyloplasts were able to relocate to the bottom of the cell and move up to 30 μm (Fig. 4E, rotation). These data confirm that altering vacuolar membrane morphology has profound effects on amyloplast movement in *zig-1*.

Wortmannin treatment of *zig-1* statocytes partially restores gravitropism

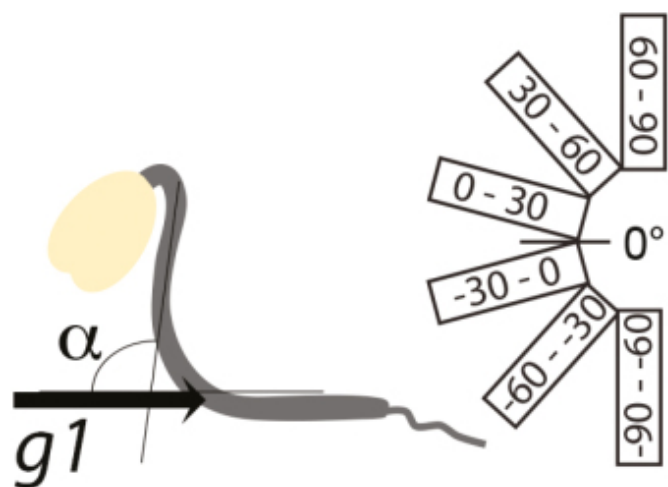
We have shown above that statocytes in the *Arabidopsis* hypocotyl may be located just below the hook (Fig. 1). To confirm this, we took advantage of the effect of Wm on *zig-1* vacuoles and amyloplast sedimentation (Fig. 4). Thus, we tested whether local Wm application to either the top or bottom of the hypocotyl was sufficient to restore gravity response in *zig-1*. A small dot of growth medium containing either 1% (v/v) DMSO (control) or 33 μM Wm was placed over the top or the bottom of the hypocotyl. The plates were then rotated 90° from the original gravity vector and the

angle of hypocotyl curvature (α) was measured after 20 h ([Fig. 5A](#)). Col-0 WT responded to the new gravity vector when DMSO (control) was placed at the top of the hypocotyls, while *zig-1* displayed an agravitropic response, as expected ([Fig. 5B](#)). When medium containing Wm was placed at the top of Col-0 hypocotyls, it induced a slight delay in graviresponse as indicated by an increase in the seedlings with an angle between 0 and 30° and a decrease in those between 30 and 60°. However, local application of Wm to the top of *zig-1* hypocotyls resulted in an enhanced response to gravity. *zig-1* mutants treated with DMSO showed a strong agravitropic phenotype, with most seedlings in the –30 to 0° and 0 to 30° categories, while *zig-1* mutants treated with Wm at the top showed an increase in the hypocotyls between 30 and 60° and a decrease in those between –30 and 0° ([Fig. 5B](#)). These results indicate that Wm application to the upper hypocotyl partially suppresses the agravitropic phenotype of *zig-1* mutants. In contrast, application of Wm to the bottom of the hypocotyl did not have major effects on gravity response in *zig-1* (see [Supplementary Fig. S2](#)). Therefore, only local Wm application to the top of *zig-1* hypocotyls can enhance their gravitropic response.

Fig. 5.

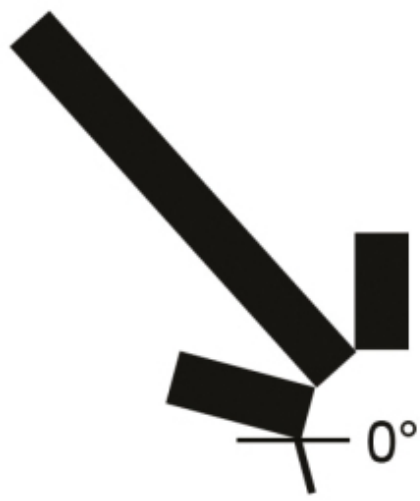
A

top bottom

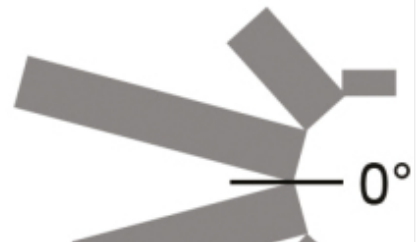
**B**

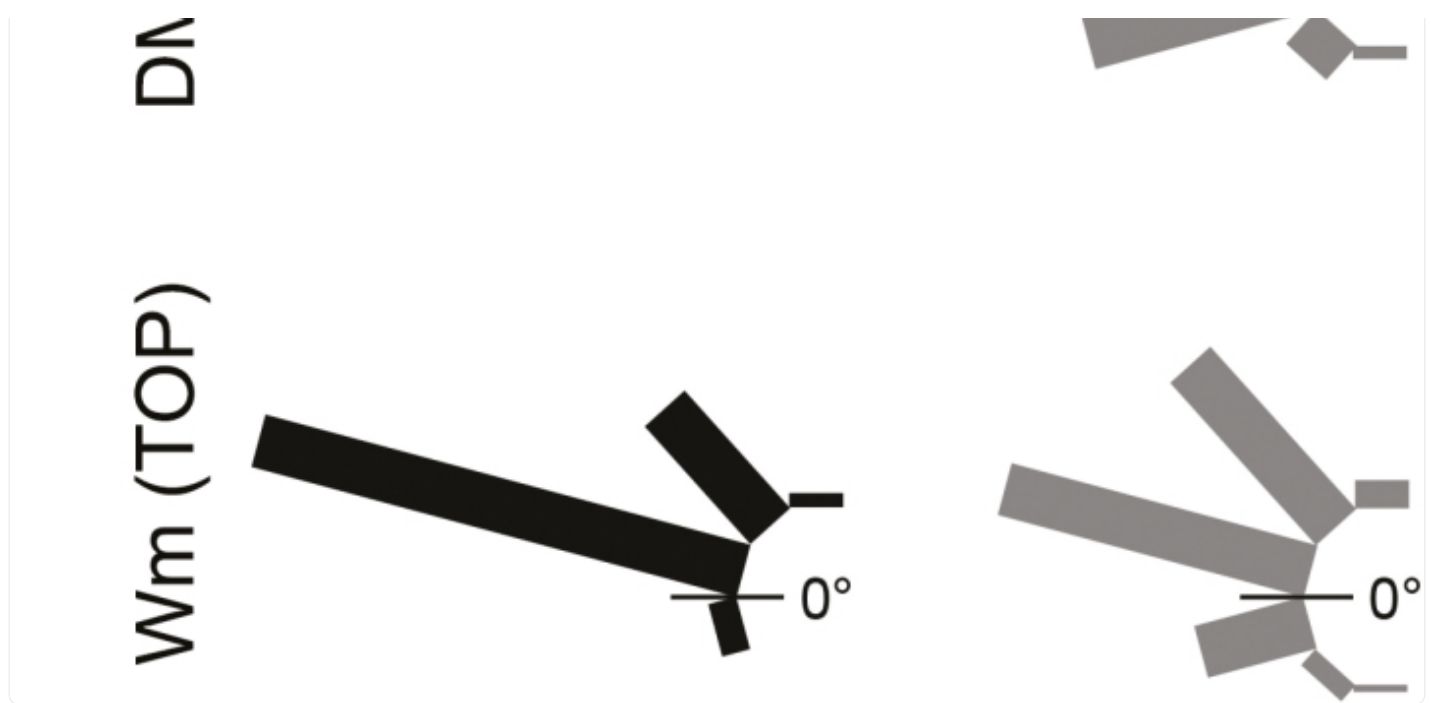
MSO (TOP)

WT



zig-1





[Open in a new tab](#)

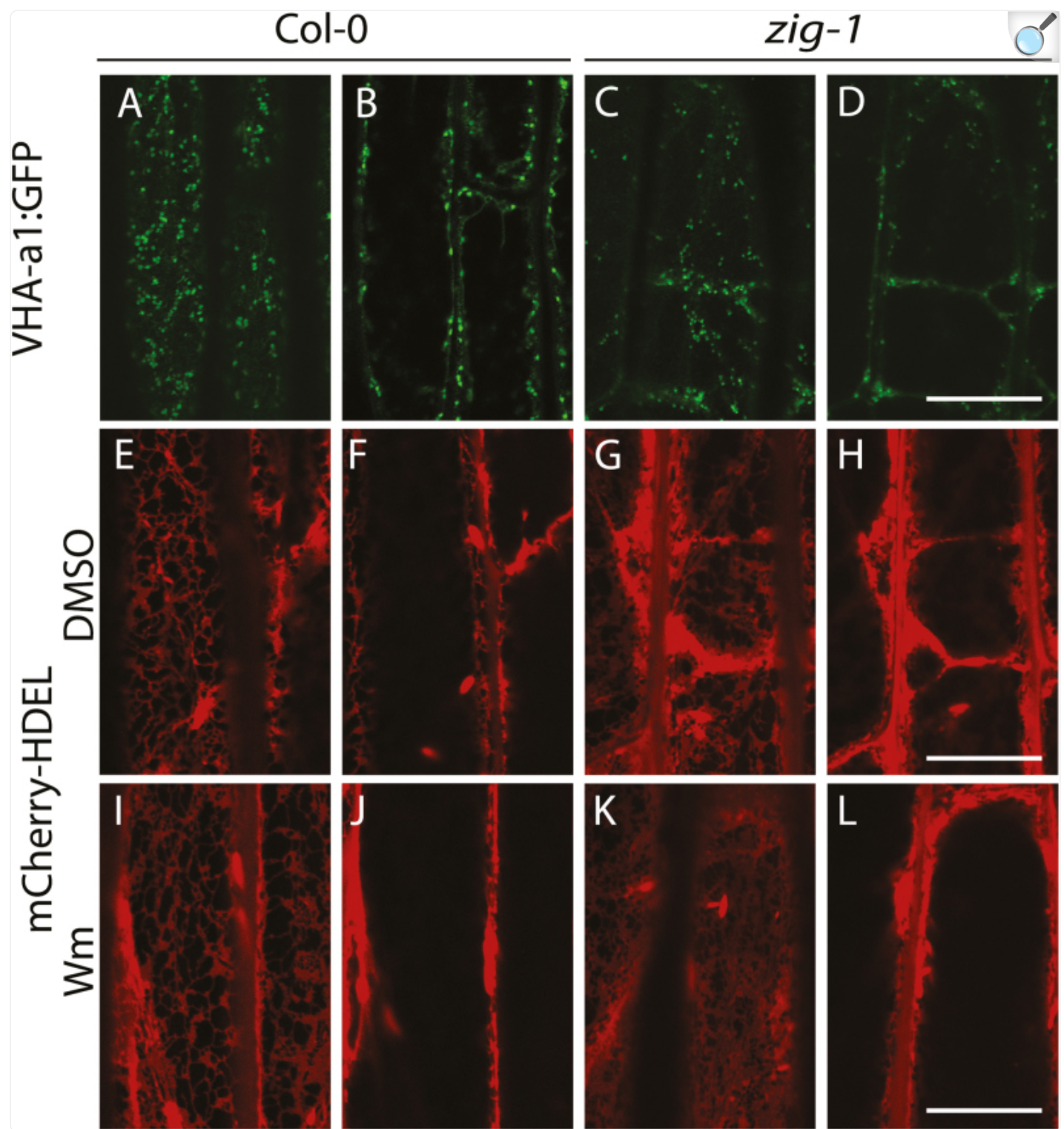
Local Wm application at the top of hypocotyls enhances gravitropism of *zig-1*. Three-day-old seedlings from Col-0 WT and *zig-1* were treated at either the top or the bottom of the hypocotyl with a dot of AGM containing DMSO or 33 µM Wm. Seedlings were then exposed to a 90° rotation, and the angle of hypocotyl curvature was measured after 20 h. (A) Illustrations showing the placement of medium dots containing DMSO or Wm at either the top or the bottom of hypocotyls, the angle of hypocotyl curvature between the first gravity vector (g_1) and the top of the hypocotyl, and how the angle distributions are represented. (B) Application of Wm at the top of the hypocotyl enhances *zig-1* gravitropism. Shown are the angle distributions for WT and *zig-1* treated with DMSO or Wm at the top of the hypocotyl ($n=87-112$). (This figure is available in color at *JXB* online.)

Loss of *VTI11* has dramatic consequences for endoplasmic reticulum organization

The dramatic restriction on amyloplast movement in *zig-1* prompted us to determine if fragmented vacuoles altered the morphology of organelles of the endomembrane system, which could impede their flow. To this end, VHA-a1-GFP, a marker for the *trans*-Golgi network (TGN) (Dettmer *et al.*, 2006), and mCherry-HDEL, a marker for the endoplasmic reticulum (ER) (Nelson *et al.*, 2007), were analysed in the *zig-1* background. Organelle morphology was analysed in hypocotyl cortical cells given the weak fluorescence of these markers in the endodermis. VHA-a1-GFP labeled typical TGN structures in WT and the *zig-1* background (Fig. 6A–D). Not surprisingly, TGN puncta were found both in the cell cortex and in the cytosol that surrounded fragmented vacuoles of *zig-1* (Fig. 6C, D). Therefore, loss of *VTI11* does not appear to have an effect on TGN morphology. The mCherry-HDEL marker showed the canonical ER network

organization at the cell cortex and ER bodies in WT ([Nelson et al., 2007](#)) ([Fig. 6E](#), F). The ER was found surrounding the small vacuoles of *zig-1*, similar to the other organelles, but two distinct abnormalities could be detected. First, the cortical organization of the ER was altered as there was enrichment of ER membranes in the cortical domains that abutted juxtaposed vacuoles ([Fig. 6G](#)). In addition, aggregates of ER were found in the cytosolic domains between juxtaposed vacuoles and these appear to have restrictions in their movement ([Fig. 6H](#) and [Supplementary Movies S1 and S2](#)). These aggregates of ER could result from accumulation of fusiform bodies at these sites, in addition to aggregated ER membranes, but these are difficult to differentiate at the resolution of a light microscope. These defects indicate that vacuole morphology is important for proper ER organization. To further test this possibility, we determined whether Wm treatment of *zig-1* would restore the cortical ER organization by promoting vacuole fusion. There were no apparent changes to the ER network in WT hypocotyls after treatment with Wm ([Fig. 6I, J](#)), although membrane aggregates were sometimes observed. As expected, Wm treatment induced the fusion of vacuoles in *zig-1*, and the enrichment of ER membranes was no longer observed in the cortex after a 2 h washout ([Fig. 6K, L](#)). These results overall indicate that vacuole morphology defects in *zig-1* do not alter the morphology of the TGN, but it does have a dramatic effect on the organization of the ER.

Fig. 6.



[Open in a new tab](#)

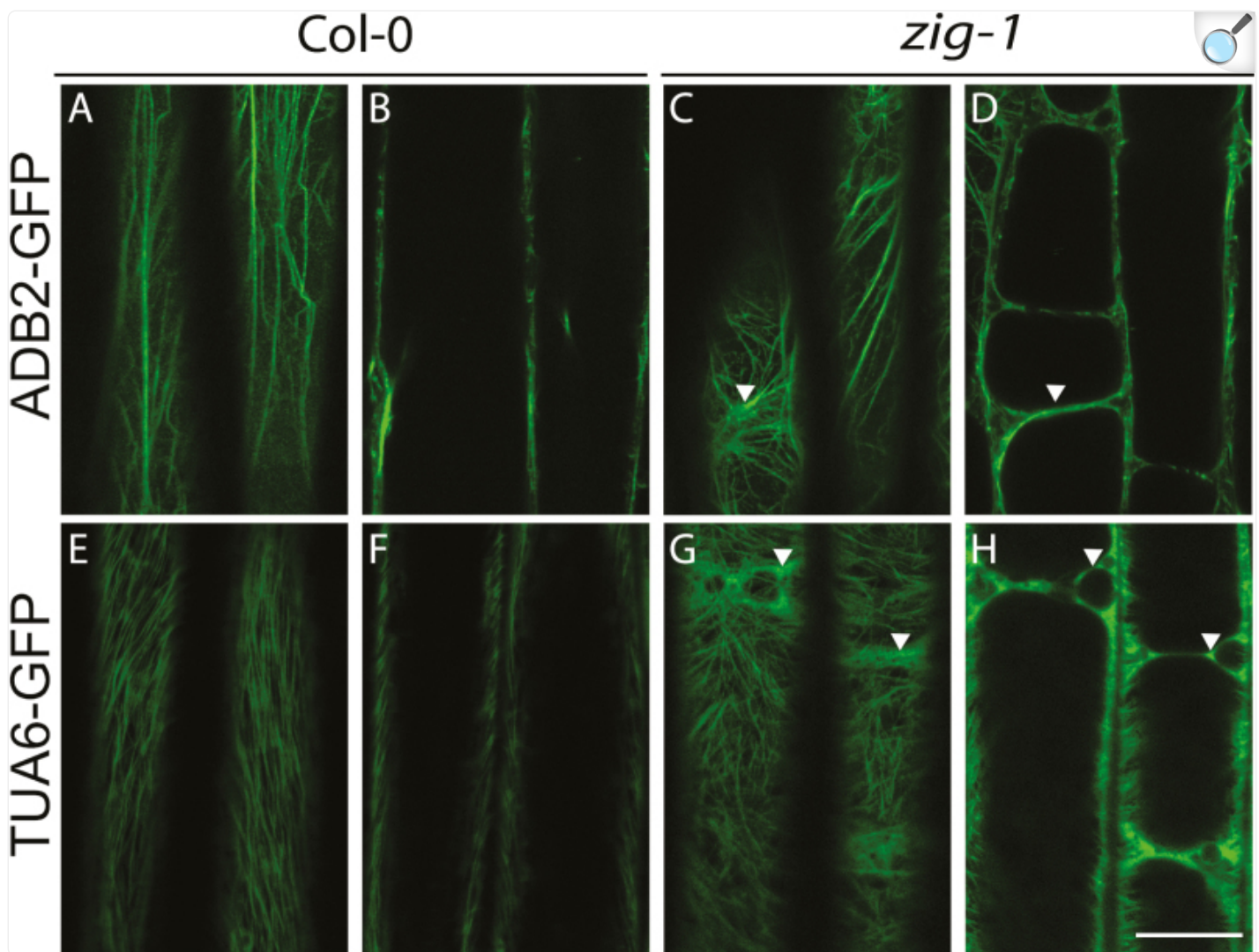
Loss of *VT111* function results in impaired ER morphology. Hypocotyl cells from 3-d-old seedlings from

Col-0 wild-type or *zig-1* expressing subcellular markers were imaged by confocal microscopy. Seedlings were grown in the dark. A cortical section and a medial section of the same cell are shown for each marker. (A–D) Col-0 wild-type or *zig-1* expressing VHA-a1-GFP. (E–L) Dark-grown Col-0 WT or *zig-1* seedlings expressing the ER marker mCherry-HDEL were treated with 1% (v/v) DMSO (E–H) or 33 µM Wm (I–L) for 3 h and then transferred to AGM for 2 h before imaging. Identical microscope settings were used for both genotypes. Scale bar: 20 µm.

Vacuoles and amyloplasts associate by cytoskeleton-independent mechanisms

F-actin is involved in amyloplast saltatory movements in wild-type ([Saito et al., 2005](#); [Yamamoto and Kiss, 2002](#)), and it may function as a negative regulator of sedimentation ([Nakamura et al., 2011](#)), but its specific role in the gravity response is unknown ([Blancaflor, 2013](#)). Because amyloplasts appear trapped between fragmented vacuoles in *zig-1* ([Fig. 1](#)) and are relatively static ([Fig. 2](#)), it was important to investigate if F-actin or microtubules were involved in restricting their movement. The cytoskeleton was visualized using the F-actin marker ABD2-GFP ([Wang et al., 2004](#)) or microtubule (MT) marker TUA6-GFP ([Ueda et al., 1999](#)) in cortical and medial sections of epidermal cells ([Fig. 7](#)). F-actin cables were observed at the cortex in *zig-1* ([Fig. 7C](#)) similar to the WT ([Fig. 7A](#)), except that the F-actin network surrounds the fragmented vacuoles in *zig-1* ([Fig. 7C](#)). We conclude that the fragmented vacuoles in *zig-1* do not impede F-actin polymerization or cortical arrangement. Similarly, microtubules were detected in the cell cortex in WT ([Fig. 7E](#)) and *zig-1* ([Fig. 7G](#)). However, dense MT arrays were also observed close to juxtaposing vacuoles ([Fig. 7H](#)). Overall, the lack of a central vacuole in *zig-1* does not appear to cause aggregates or abnormalities in the composition of the cytoskeletal network, except that both polymers are found surrounding the *zig-1* vacuoles.

Fig. 7.



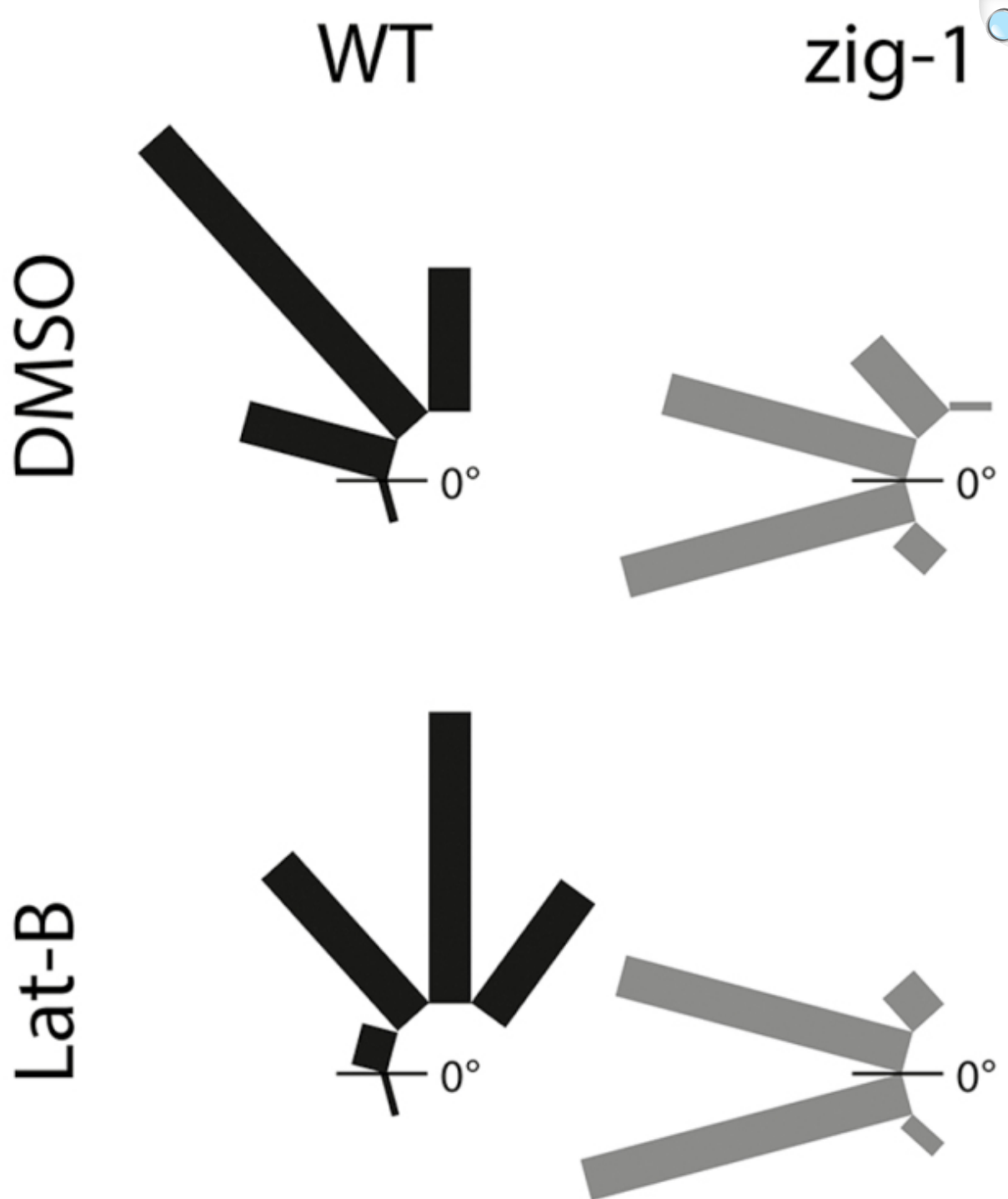
[Open in a new tab](#)

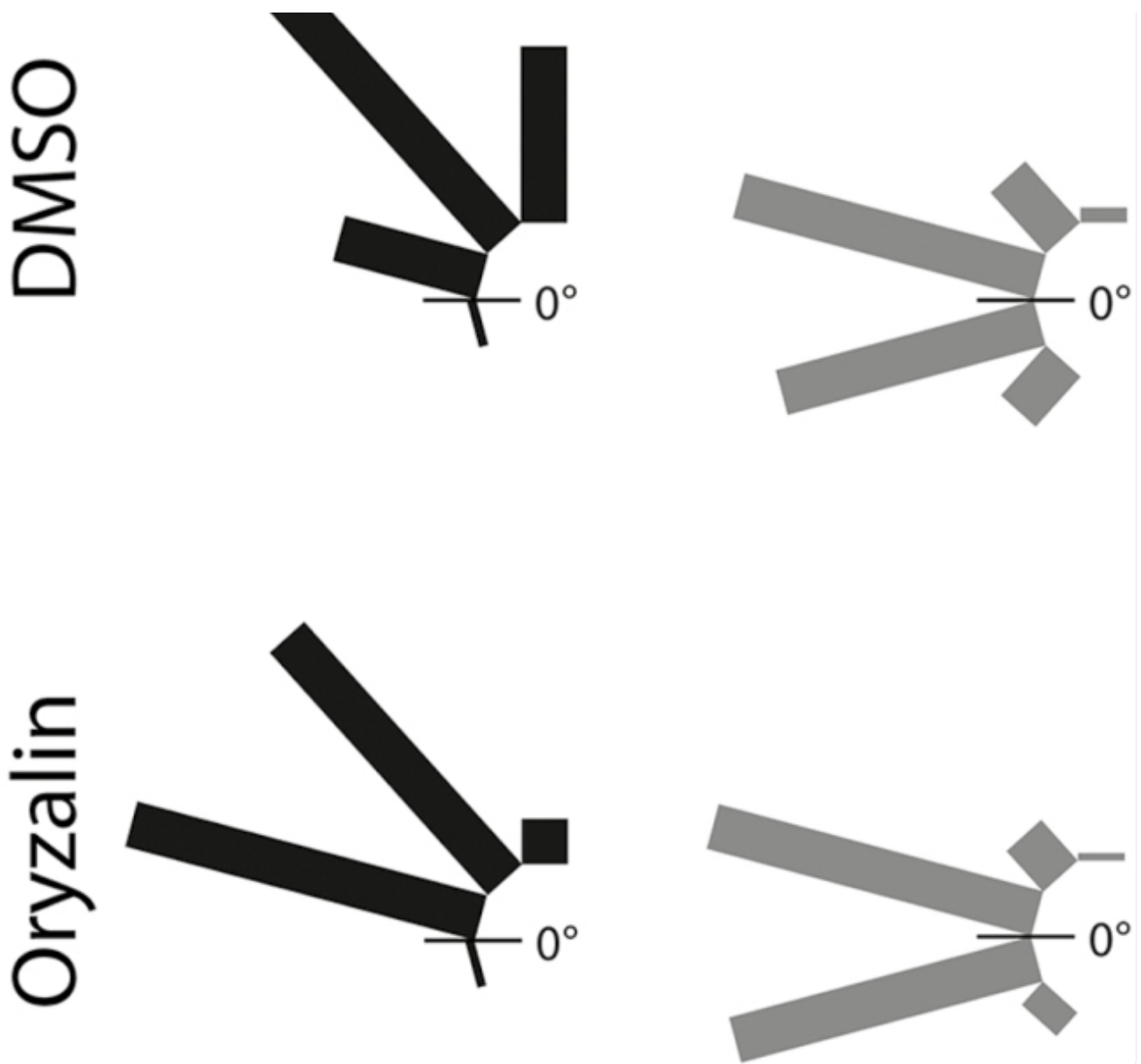
The cytoskeleton organization at the cortex is not affected in *zig-1*. Four-day-old seedlings from Col-0 WT (A, B, E, F) or *zig-1* (C, D, G, H) expressing ABD2-GFP to label F-actin (A–D) or TUA6-GFP to label microtubules (E–H) were imaged by confocal microscopy. Both cortical sections (A, C, E, G) and medial sections (B, D, F, H) for a representative cell are shown. Seedlings were grown in the dark. Arrowheads indicate zones with cytoskeleton enrichment that are found above juxtaposing vacuoles. Scale bar: 20 μ m. (This figure is available in color at *JXB* online.)

We conducted gravitropic assays in the presence and absence of the cytoskeleton inhibitors lantrunculin B (Lat-B) or oryzalin to determine if the cytoskeleton contributed to the static behavior of *zig-1* amyloplasts. Lat-B induced an

increase in the response to gravity in WT including an increase in the hypocotyls between 60 and 90° and hypocotyl curvatures of more than 90° in 22.1% of seedlings ([Fig. 8A](#)). No changes were observed in *zig-1*, with or without Lat-B, as most *zig-1* hypocotyls were found in two categories, –30 to 0° and 0 to 30°, in both treatments ([Fig. 8A](#)). The ABD2-GFP marker was included in these experiments as a control to show the effectiveness of the Lat-B treatment (see [Supplementary Fig. S3A](#)). A possible role of MT in tethering of amyloplasts was also tested ([Fig. 8B](#)). There was a delay in the response of the oryzalin-treated seedlings, with an increase in the proportion of seedlings in the 0–30° category and a decrease in the 60–90° category. In the case of *zig-1*, both treatments resulted in very similar angle distributions, with almost all seedlings bending to an angle between –30 and 30°. Therefore, treatment with oryzalin does not enhance graviresponse of *zig-1*. Again, the TUA6-GFP marker was used to confirm the effectiveness of the oryzalin treatment ([Supplementary Fig. S3C](#)).

Fig. 8.

A**B**



[Open in a new tab](#)

Neither lantrunculin B (Lat B) nor oryzalin treatment suppresses the agravitropic phenotype of *zig-1*. Gravitropism assay with Col-0 WT and *zig-1* in the presence of cytoskeleton inhibitors. Seedlings were grown vertically for 3 d in the dark, and then transferred to AGM plates containing 1% (v/v) DMSO (A, B), 2 μ M Lat-B (A) or 20 μ M oryzalin (B). Plates were returned to the dark and oriented at 90° from the original gravity vector (g1). After 20 h the angle of hypocotyl curvature was measured between g1 and the top of the hypocotyl. The distribution of seedlings in each degree class is indicated. $n=77-100$.

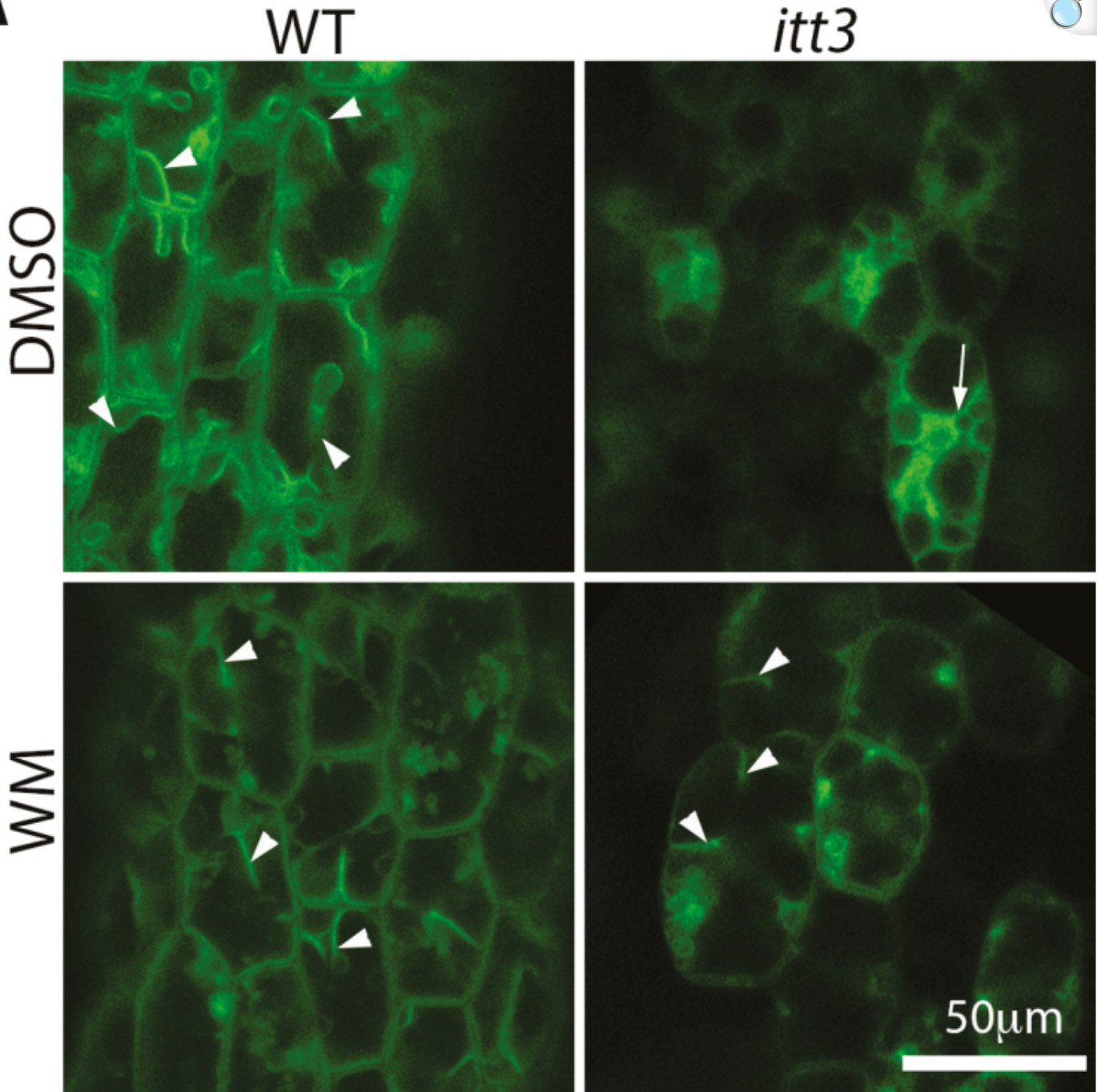
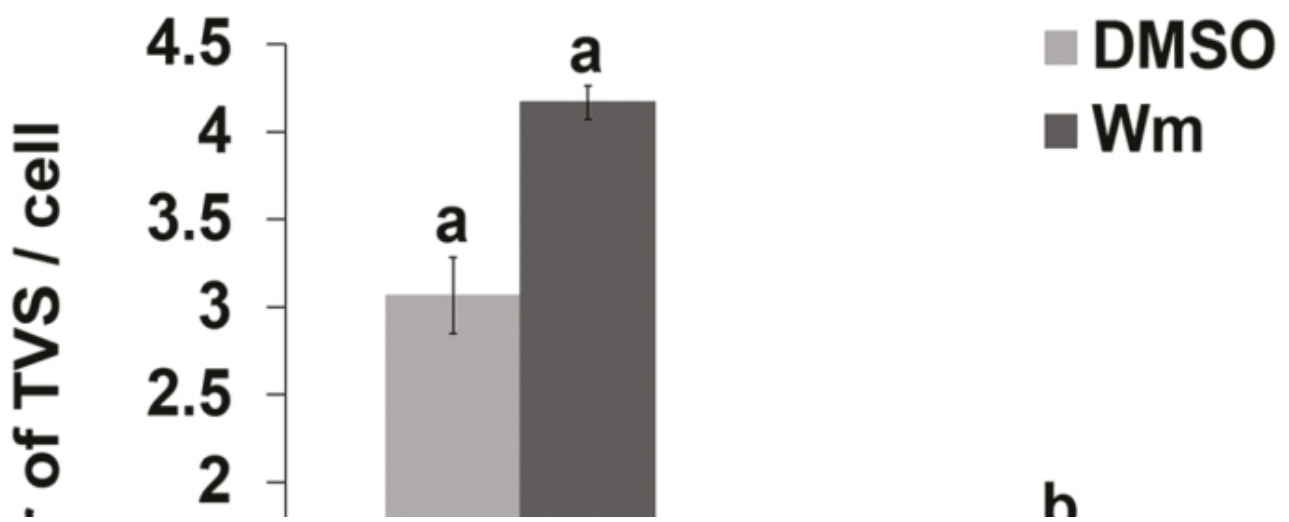
That neither Lat-B nor oryzalin treatments suppressed the agravitropic phenotype of *zig-1* suggested that neither actin nor MT depolymerization was sufficient to release amyloplasts from the static inter-vacuolar junctions. To confirm this, amyloplast sedimentation was visualized after inhibitor treatment in the endodermis of dark-grown hypocotyls (see [Supplementary Fig. S3B](#)). In this experiment, seedlings were incubated overnight in the presence of DMSO, 2 μ M

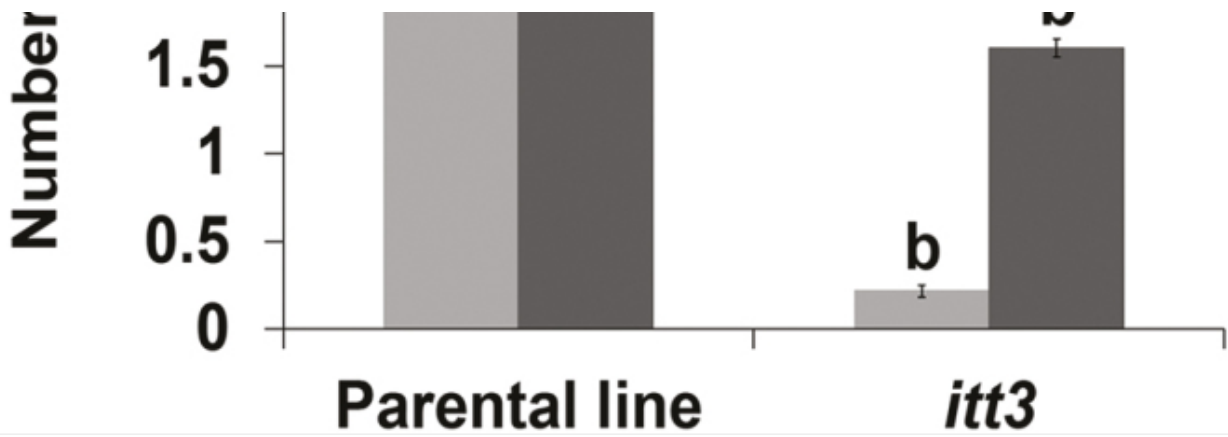
Lat-B or 20 μ M oryzalin to depolymerize the cytoskeleton. Seedlings were then incubated vertically for 10 min, imaged, incubated vertically again for 10 min but upside down (180° rotation), and then imaged again. Wild-type amyloplasts sedimented to the new bottom of the cell after the 180° rotation regardless of chemical pretreatment. In contrast, *zig-1* amyloplasts did not sediment in either of the chemical treatments as shown by their static localization before and after reorientation ([Supplementary Fig. S3B](#)). Since depolymerization of F-actin or MT does not enhance gravity response in *zig-1*, nor does it restore amyloplast sedimentation, these results overall indicate that actin filaments or microtubules are not contributing to the immobile nature of amyloplasts by serving as a physical tether connecting amyloplasts and tonoplast. Therefore, the static nature of *zig-1* amyloplasts is not explained by physical associations with the cytoskeleton.

Wm enhances graviresponse of *vti11* alleles through dynamic TVS formation

We have demonstrated that immobile amyloplasts in *zig-1* hypocotyls increase dynamic movements after Wm treatments. We then quantified transvacuolar strands (TVSs) in hypocotyls of WT and *itt3* before and after Wm treatment ([Fig. 9A](#)) to test whether this enhanced motion is due to vacuolar membrane remodeling through changes in TVS formation. The parental line showed 3.07 ± 0.22 TVSs per cell in hypocotyl epidermis, while *itt3* mutants had only 0.22 ± 0.04 TVSs when DMSO treatments were used ([Fig. 9B](#)). The number of TVSs increased to 4.17 ± 0.10 in the parental line and to 1.60 ± 0.05 for *itt3* when seedlings were treated with Wm for 2 h. The significant increase in the number of TVSs after Wm treatment for both the parental line and *itt3* suggests that Wm not only promotes vacuole fusion, but has a positive effect on vacuole membrane dynamics as well.

Fig. 9.

A**B**



[Open in a new tab](#)

Wm treatment induces the formation of transvacuolar strands (TVSs). (A) Thick optical sections were captured for TVS quantification at low magnification. Example images used from WT and *itt3* hypocotyls are shown for both DMSO and Wm treatments. The types of TVS that were counted are indicated with arrowheads. Note that membranes that fully surrounded a vacuole in *itt3* were not included (arrows). (B) Average number of TVSs per cell in parental and *itt3*. $n=60$ cells total from four seedlings per genotype. Mean values are statistically significant (Student's *t* test, two tailed, $P\leq 0.05$) if letters are different.

Discussion

Here, we used live-cell imaging to analyse the dynamics of amyloplast sedimentation in *Arabidopsis* hypocotyls from whole seedlings. Previous studies have utilized cuttings from inflorescence stems ([Morita et al., 2002](#); [Saito et al., 2005](#); [Toyota et al., 2013b](#)). Our microscope set-up allowed us to image endodermis through the almost transparent cortex of etiolated hypocotyls using a fluorescence microscope. A very small amount of Immersol allowed us to use a water immersion objective on the vertical stage, which provided optimal resolution. This unique set-up allowed us to track amyloplast sedimentation in real time and in whole plants without the concerns of plant injury. The system is amenable for cell biology analysis, including treatment with chemical inhibitors, and long-term time-lapse experiments. Furthermore, this system can overcome the challenges of imaging using stem cuttings, which have been shown to affect the vacuole morphology of certain mutants ([Hashiguchi et al., 2014](#)). One caveat of our system is the need to illuminate the seedlings during image acquisition, which we have addressed with a green filter to minimize phototropic responses. Green light, however, has been shown to enhance hypocotyl growth and inhibit blue and red phototropic responses in dark-grown seedlings ([Folta, 2004](#); [Folta and Maruhnich, 2007](#); [McCoshum and Kiss, 2011](#)). Therefore, experiments in the vertical stage must be interpreted with caution as they may be influenced by effects of the green light on seedling growth.

Restriction of amyloplast sedimentation in *zig-1* is dependent on its vacuole

phenotype

A role for the vacuole in gravity perception or response is well documented ([Morita et al., 2002](#); [Yano et al., 2003](#); [Saito et al., 2005](#)). The *VT111* loss of function mutant *sgr4/zig-1* was originally identified for its agravitropic phenotype in shoots ([Yamauchi et al., 1997](#); [Kato et al., 2002](#)), and it was later shown to display abnormal vacuole morphology and reduced vacuole fusion ([Zheng et al., 2014b](#)). We used *zig-1* and a second allele, *itt3*, as tools to interrogate the role of vacuole dynamics on gravitropism in *Arabidopsis* hypocotyls. As expected, WT endodermal cells from hypocotyl statocytes show a large central vacuole and sedimented amyloplasts that appeared surrounded by tonoplast membrane. This organization is very similar to that found in inflorescence stems ([Morita et al., 2002](#)). In contrast, and consistent with other tissues ([Zheng et al., 2014a,b](#)), smaller unfused vacuoles were detected in endodermal statocytes from *zig-1* mutants, where the amyloplasts were found distributed almost randomly throughout the cell. In these cells, amyloplasts appeared trapped at the junction of juxtaposing vacuoles, and this organization seems to prevent amyloplast movement in *zig-1*, both before and after gravistimulation, as depicted by time-lapse experiments. Surprisingly, conditions of hypergravity up to 10 g were not sufficient to force amyloplasts to sediment in these cells. It is unlikely that the fragmented vacuoles alone would be sufficient to prevent the movement of these organelles simply by creating physical obstacles to their movements along the cytosolic space. Therefore, we propose that a physical tether exists between the vacuole and amyloplasts that is of sufficient strength to resist a 10 g force. In fact in the case of *zig-1*, each amyloplast seems attached to multiple vacuoles, which perhaps generates a strong physical tethering structure to resist this hypergravity pull. In contrast, hypergravity is known to increase amyloplast sedimentation and gravitropic curvature of other agravitropic mutants such as *sgr2*, *sgr9*, and *pgm* ([Toyota et al., 2013b](#)), but none of these mutants displays a fragmented vacuole phenotype. Amyloplast sedimentation has been shown to occur via transvacuolar strands ([Morita et al., 2002](#); [Saito et al., 2005](#)), and therefore we asked whether the fragmented vacuole phenotype of *zig-1* could impair TVS formation. In fact, *zig-1* mutants formed very few TVS structures in epidermal cells when compared with the WT, which could contribute to the reduced sedimentation of amyloplasts inside their statocytes. This possibility is consistent with the phenotype of the *sgr2* mutant, which displays fewer TVSs than WT and is agravitropic ([Morita et al., 2002](#); [Saito et al., 2005](#)).

Treatment with Wm induces fusion and restores the vacuole morphology of *zig-1* ([Zheng et al., 2014a,b](#)). We used this assay to test whether the vacuole morphology phenotype of *zig-1* was necessary for their lack of amyloplast sedimentation and the role of vacuole morphology on this movement. As expected, Wm treatment increased amyloplast sedimentation in *zig-1*. The Wm-induced vacuole fusion may have this effect due to the following: (i) vacuole fusion could disrupt the putative tethers between amyloplasts and the vacuolar membrane proposed above and therefore increase mobility of these organelles; (ii) vacuole fusion could restore the ability to form TVSs, which could become conduits for amyloplast sedimentation; (iii) restoring the single vacuole phenotype could remove physical obstacles formed by the vacuoles themselves. We indeed confirmed that Wm-induced vacuole fusion increases the formation of TVSs in epidermal cells. However, TVSs alone are probably not sufficient because *sgr2* mutants, which do not form TVSs in stems, were able to reposition amyloplasts along a hypergravity vector ([Toyota et al., 2013b](#)). Future research

is needed to address the role of a putative tethering system to determine if all three possibilities play a role in this response. The alternate possibility that Wm is actually affecting gravitropism through effects on cellular events unrelated to vacuolar function seems less likely as Wm action on gravity response is not seen in WT plants where these other sites of action would presumably still be present.

Shoot statocytes comprise young endodermal cells near the top of the hypocotyl

The endodermal layer of the hypocotyl has been identified as the graviperceptive tissue in shoots ([Fukaki et al., 1998](#)). Visualization of endodermal cells in the medial region of the hypocotyl of etiolated seedlings indicated that most cells did not show the expected sedimented amyloplasts, and instead these organelles were in constant motion from cytoplasmic streaming. Only the smaller cells in the upper hypocotyl of an average length of 70 μm or less showed sedimented amyloplasts that were consistent with graviperception. To confirm this result, we took advantage of the phenotype of *zig-1* and Wm treatment. This provided a unique opportunity to test whether amyloplast sedimentation in *zig-1* at the top or the bottom of the hypocotyl was associated with restoration of gravitropism. Adding Wm at the top of the hypocotyl enhanced gravitropism in these mutants, but the treatment at the bottom did not. Therefore, only Wm treatment at the top is sufficient to restore the gravity response. This effect is correlated with an increase in amyloplast sedimentation as shown by organelle tracking experiments. Altogether, these results indicate that the statocytes in etiolated hypocotyls are localized to the young endodermal cells at the top of the hypocotyl. These results are consistent with the top ~4 cm region of the inflorescence stem being sufficient for graviresponse in mature plants ([Fukaki et al., 1996a](#)) and the finding that displacement of amyloplasts at the base of the inflorescence stem does not result in inflorescence bending ([Weise et al., 2000](#)).

The cytoskeleton is not involved in amyloplast tethering to *zig-1* vacuoles

A role for actin during shoot gravitropic perception remains unclear ([Yamamoto and Kiss, 2002](#); [Yamamoto et al., 2002](#); [Palmieri and Kiss, 2005](#); [Saito et al., 2005](#); [Blancaflor, 2013](#)). The inability of amyloplasts to sediment in *zig-1* could be due to the fragmented vacuoles being obstacles for movement. However the fact that hypergravity is not sufficient to release them indicates that there may be physical tethers between the amyloplasts and the vacuole. We tested whether such tethers could be formed in part by cytoskeletal structures and, therefore, if they could be disrupted with inhibitors that depolymerize MT and actin microfilaments. However, neither Lat-B nor oryzalin treatment was sufficient to overcome the block in sedimentation. This is consistent with previous reports indicating that the tight association between vacuole and amyloplasts was not disrupted by lantrunculin B in wild-type inflorescences ([Saito et al., 2005](#)). However, these results are not consistent with experiments in flowering snapdragon shoots, in which depolymerization of actin microfilaments with Lat-B released amyloplasts ([Friedman et al., 2003](#)). We conclude that the association between amyloplasts and the vacuole may occur either directly or indirectly but does not seem to involve the cytoskeleton. Contact sites between the vacuole and other organelles and association between those and amyloplasts may be responsible for the tethering that we have observed. Contact sites between plant subcellular organelles have been

identified by electron microscopy or laser trapping, including between ER and plasma membrane (summarized in [Staehelin, 1997](#)), ER and endosomes ([Stefano et al., 2015](#)), and ER and Golgi ([Sparkes et al., 2009](#)). The vacuole has also been shown in tight association with the cytoskeleton ([Scheuring et al., 2016](#)) and the ER ([Staehelin, 1997](#)), and the latter may provide an anchoring system that may be important to regulate amyloplast sedimentation. Future analysis by electron microscopy in shoot endodermal cells may provide further support for these contact sites. The dramatic effects on ER morphology in the *zig-1* mutant indicates that ER–vacuole interactions are critical for organelle structure. Given that no major changes in organelle morphology or distribution were observed for the TGN, we conclude that the vacuole is unlikely to form physical attachments with these organelles as it does for amyloplasts.

Supplementary data

Supplementary data are available at *JXB* online.

[Fig. S1](#) . Microscope set-up for live-cell imaging with a vertical stage and a sample chamber.

[Fig. S2](#) . Local Wm application at the bottom of hypocotyls does not enhance gravitropism of *zig-1*.

[Fig. S3](#) . Lat-B and oryzalin depolymerize cytoskeleton, but do not free amyloplasts in the *zig-1* background.

[Movie S1](#) . Time lapse of the ER marker mCherry-HDEL in dark-grown Col-0 WT.

[Movie S2](#) . Time lapse of the ER marker mCherry-HDEL in dark-grown *zig-1*.

Supplementary Data

[supp_67_22_6459_index.html](#) (1.1KB, html)

Acknowledgements

The authors thank E. Blancaflor (Noble Foundation) for the ABD2-GFP marker line, R. Sozanni for the pSCR2.0 clone, W. Guevara for technical assistance, D. Carter for helpful discussions, and J. Stewart for assistance with graphics. This work was supported by NASA Space Life and Physical Sciences Division (NNX13AM49G to MRP and NNX14AT25G to SG), National Science Foundation (MCB-1244354 to MRP) and JST (PRESTO award to MT).

References

1. Behera S, Kudla J. 2013. Live cell imaging of cytoplasmic Ca²⁺ dynamics in Arabidopsis guard cells. *Cold Spring Harbor Protocols* 2013, 665–669. [[DOI](#)] [[PubMed](#)] [[Google Scholar](#)]
2. Blancaflor EB. 2013. Regulation of plant gravity sensing and signaling by the actin cytoskeleton. *American Journal of Botany* 100, 143–152. [[DOI](#)] [[PubMed](#)] [[Google Scholar](#)]
3. Blancaflor EB, Masson PH. 2003. Plant gravitropism. Unraveling the ups and downs of a complex process. *Plant Physiology* 133, 1677–1690. [[DOI](#)] [[PMC free article](#)] [[PubMed](#)] [[Google Scholar](#)]
4. Chen YA, Scheller RH. 2001. SNARE-mediated membrane fusion. *Nature Reviews Molecular Cell Biology* 2, 98–106. [[DOI](#)] [[PubMed](#)] [[Google Scholar](#)]
5. Clough SJ, Bent AF. 1998. Floral dip: a simplified method for Agrobacterium-mediated transformation of *Arabidopsis thaliana*. *The Plant Journal* 16, 735–746. [[DOI](#)] [[PubMed](#)] [[Google Scholar](#)]
6. Dettmer J, Hong-Hermesdorf A, Stierhof YD, Schumacher K. 2006. Vacuolar H⁺-ATPase activity is required for endocytic and secretory trafficking in *Arabidopsis*. *The Plant Cell* 18, 715–730. [[DOI](#)] [[PMC free article](#)] [[PubMed](#)] [[Google Scholar](#)]
7. Fitzelle KJ, Kiss JZ. 2001. Restoration of gravitropic sensitivity in starch-deficient mutants of *Arabidopsis* by hypergravity. *Journal of Experimental Botany* 52, 265–275. [[PubMed](#)] [[Google Scholar](#)]
8. Folta KM. 2004. Green light stimulates early stem elongation, antagonizing light-mediated growth inhibition. *Plant Physiology* 135, 1407–1416. [[DOI](#)] [[PMC free article](#)] [[PubMed](#)] [[Google Scholar](#)]
9. Folta KM, Maruhnich SA. 2007. Green light: a signal to slow down or stop. *Journal of Experimental Botany* 58, 3099–3111. [[DOI](#)] [[PubMed](#)] [[Google Scholar](#)]
10. Friedman H, Vos JW, Hepler PK, Meir S, Halevy AH, Philosoph-Hadas S. 2003. The role of actin filaments in the gravitropic response of snapdragon flowering shoots. *Planta* 216, 1034–1042. [[DOI](#)] [[PubMed](#)] [[Google Scholar](#)]
11. Fujihira K, Kurata T, Watahiki MK, Karahara I, Yamamoto KT. 2000. An agravitropic mutant of *Arabidopsis*, endodermal-amyo plast less 1, that lacks amyloplasts in hypocotyl endodermal cell layer. *Plant and Cell Physiology* 41, 1193–1199. [[DOI](#)] [[PubMed](#)] [[Google Scholar](#)]
12. Fukaki H, Fujisawa H, Tasaka M. 1996. *a* Gravitropic response of inflorescence stems in *Arabidopsis thaliana*. *Plant Physiology* 110, 933–943. [[DOI](#)] [[PMC free article](#)] [[PubMed](#)] [[Google Scholar](#)]
13. Fukaki H, Fujisawa H, Tasaka M. 1996. *b* SGR1, SGR2, SGR3: novel genetic loci involved in shoot

- gravitropism in *Arabidopsis thaliana*. *Plant Physiology* 110, 945–955. [[DOI](#)] [[PMC free article](#)] [[PubMed](#)] [[Google Scholar](#)]
14. Fukaki H, Wysocka-Diller J, Kato T, Fujisawa H, Benfey PN, Tasaka M. 1998. Genetic evidence that the endodermis is essential for shoot gravitropism in *Arabidopsis thaliana*. *The Plant Journal* 14, 425–430. [[DOI](#)] [[PubMed](#)] [[Google Scholar](#)]
15. Gao XQ, Li CG, Wei PC, Zhang XY, Chen J, Wang XC. 2005. The dynamic changes of tonoplasts in guard cells are important for stomatal movement in *Vicia faba*. *Plant Physiology* 139, 1207–1216. [[DOI](#)] [[PMC free article](#)] [[PubMed](#)] [[Google Scholar](#)]
16. Han SW, Alonso JM, Rojas-Pierce M. 2015. REGULATOR OF BULB BIOGENESIS1 (RBB1) is involved in vacuole bulb formation in *Arabidopsis*. *PLoS ONE* 10, e0125621. [[DOI](#)] [[PMC free article](#)] [[PubMed](#)] [[Google Scholar](#)]
17. Hashiguchi Y, Tasaka M, Morita MT. 2013. Mechanism of higher plant gravity sensing. *American Journal of Botany* 100, 91–100. [[DOI](#)] [[PubMed](#)] [[Google Scholar](#)]
18. Hashiguchi Y, Yano D, Nagafusa K, Kato T, Saito C, Uemura T, Ueda T, Nakano A, Tasaka M, Morita MT. 2014. A unique HEAT repeat-containing protein SHOOT GRAVITROPISM6 is involved in vacuolar membrane dynamics in gravity-sensing cells of *Arabidopsis* inflorescence stem. *Plant and Cell Physiology* 55, 811–822. [[DOI](#)] [[PMC free article](#)] [[PubMed](#)] [[Google Scholar](#)]
19. Jung JY, Kim YW, Kwak JM, Hwang JU, Young J, Schroeder JI, Hwang I, Lee Y. 2002. Phosphatidylinositol 3- and 4-phosphate are required for normal stomatal movements. *The Plant Cell* 14, 2399–2412. [[DOI](#)] [[PMC free article](#)] [[PubMed](#)] [[Google Scholar](#)]
20. Kato T, Morita MT, Fukaki H, Yamauchi Y, Uehara M, Niihama M, Tasaka M. 2002. SGR2, a phospholipase-like protein, and zig/sgr4, a SNARE, are involved in the shoot gravitropism of *Arabidopsis*. *The Plant Cell* 14, 33–46. [[DOI](#)] [[PMC free article](#)] [[PubMed](#)] [[Google Scholar](#)]
21. Kiss JZ, Guisinger MM, Miller AJ, Stackhouse KS. 1997. Reduced gravitropism in hypocotyls of starch-deficient mutants of *Arabidopsis*. *Plant and Cell Physiology* 38, 518–525. [[DOI](#)] [[PubMed](#)] [[Google Scholar](#)]
22. Leitz G, Kang BH, Schoenwaelder ME, Staehelin LA. 2009. Statolith sedimentation kinetics and force transduction to the cortical endoplasmic reticulum in gravity-sensing *Arabidopsis* columella cells. *The Plant Cell* 21, 843–860. [[DOI](#)] [[PMC free article](#)] [[PubMed](#)] [[Google Scholar](#)]
23. Levesque MP, Vernoux T, Busch W, et al. 2006. Whole-genome analysis of the SHORT-ROOT developmental pathway in *Arabidopsis*. *PLoS Biology* 4, e143. [[DOI](#)] [[PMC free article](#)] [[PubMed](#)]

[[Google Scholar](#)]

24. McCoshum S, Kiss JZ. 2011. Green light affects blue-light-based phototropism in hypocotyls of *Arabidopsis thaliana*. *Journal of the Torrey Botanical Society* 138, 409–417. [[Google Scholar](#)]
25. Masson PH, Tasaka M, Morita MT, Guan C, Chen R, Boonsirichai K. 2002. *Arabidopsis thaliana*: A model for the study of root and shoot gravitropism. *Arabidopsis Book* 1, e0043. [[DOI](#)] [[PMC free article](#)] [[PubMed](#)] [[Google Scholar](#)]
26. Moiota MT, Nakamura M, Tasaka M. 2012. Gravity sensing, interpretation, and response. In: Witzany G, Baluška F, eds. *Biocommunication of Plants*. Berlin, Heidelberg: Springer, 51–66. [[Google Scholar](#)]
27. Morita MT. 2010. Directional gravity sensing in gravitropism. *Annual Review of Plant Biology* 61, 705–720. [[DOI](#)] [[PubMed](#)] [[Google Scholar](#)]
28. Morita MT, Kato T, Nagafusa K, Saito C, Ueda T, Nakano A, Tasaka M. 2002. Involvement of the vacuoles of the endodermis in the early process of shoot gravitropism in *Arabidopsis*. *The Plant Cell* 14, 47–56. [[DOI](#)] [[PMC free article](#)] [[PubMed](#)] [[Google Scholar](#)]
29. Nakamura M, Toyota M, Tasaka M, Morita MT. 2011. An *Arabidopsis* E3 ligase, SHOOT GRAVITROPISM9, modulates the interaction between statoliths and F-actin in gravity sensing. *The Plant Cell* 23, 1830–1848. [[DOI](#)] [[PMC free article](#)] [[PubMed](#)] [[Google Scholar](#)]
30. Nelson BK, Cai X, Nebenfuhr A. 2007. A multicolored set of *in vivo* organelle markers for co-localization studies in *Arabidopsis* and other plants. *The Plant Journal* 51, 1126–1136. [[DOI](#)] [[PubMed](#)] [[Google Scholar](#)]
31. Palmieri M, Kiss JZ. 2005. Disruption of the F-actin cytoskeleton limits statolith movement in *Arabidopsis* hypocotyls. *Journal of Experimental Botany* 56, 2539–2550. [[DOI](#)] [[PubMed](#)] [[Google Scholar](#)]
32. Rakusova H, Gallego-Bartolome J, Vanstraelen M, Robert HS, Alabadi D, Blazquez MA, Benkova E, Friml J. 2011. Polarization of PIN3-dependent auxin transport for hypocotyl gravitropic response in *Arabidopsis thaliana*. *The Plant Journal* 67, 817–826. [[DOI](#)] [[PubMed](#)] [[Google Scholar](#)]
33. Saito C, Morita MT, Kato T, Tasaka M. 2005. Amyloplasts and vacuolar membrane dynamics in the living graviperceptive cell of the *Arabidopsis* inflorescence stem. *The Plant Cell* 17, 548–558. [[DOI](#)] [[PMC free article](#)] [[PubMed](#)] [[Google Scholar](#)]
34. Scheuring D, Lofke C, Kruger F, Kittelmann M, Eisa A, Hughes L, Smith RS, Hawes C, Schumacher K, Kleine-Vehn J. 2016. Actin-dependent vacuolar occupancy of the cell determines auxin-induced growth

repression. *Proceedings of the National Academy of Sciences of the United States of America* 113, 452–457. [DOI] [PMC free article] [PubMed] [Google Scholar]

35. Sozzani R, Cui H, Moreno-Risueno MA, Busch W, Van Norman JM, Vernoux T, Brady SM, Dewitte W, Murray JAH, Benfey PN. 2010. Spatiotemporal regulation of cell-cycle genes by SHORTROOT links patterning and growth. *Nature* 466, 128–132. [DOI] [PMC free article] [PubMed] [Google Scholar]
36. Sparkes IA, Ketelaar T, De Ruijter NCA, Hawes C. 2009. Grab a Golgi: Laser trapping of Golgi bodies reveals in vivo interactions with the endoplasmic reticulum. *Traffic* 10, 567–571. [DOI] [PubMed] [Google Scholar]
37. Staehelin LA. 1997. The plant ER: a dynamic organelle composed of a large number of discrete functional domains. *The Plant Journal* 11, 1151–1165. [DOI] [PubMed] [Google Scholar]
38. Stefano G, Renna L, Lai Y, Slabaugh E, Mannino N, Buono RA, Otegui MS, Brandizzi F. 2015. ER network homeostasis is critical for plant endosome streaming and endocytosis. *Cell Discovery* 1, 15033. [DOI] [PMC free article] [PubMed] [Google Scholar]
39. Tamura K, Takahashi H, Kunieda T, Fuji K, Shimada T, Hara-Nishimura I. 2007. Arabidopsis KAM2/GRV2 is required for proper endosome formation and functions in vacuolar sorting and determination of the embryo growth axis. *The Plant Cell* 19, 320–332. [DOI] [PMC free article] [PubMed] [Google Scholar]
40. Toyota M, Ikeda N, Sawai-Toyota S, Kato T, Gilroy S, Tasaka M, Morita MT. 2013. *b* Amyloplast displacement is necessary for gravisensing in *Arabidopsis* shoots as revealed by a centrifuge microscope. *The Plant Journal* 76, 648–660. [DOI] [PubMed] [Google Scholar]
41. Toyota M, Ikeda N, Tasaka M, Morita MT. 2013. *a* Centrifuge microscopy to analyze the sedimentary movements of amyloplasts. *Bio-Protocol* 4, e1229. [Google Scholar]
42. Ueda K, Matsuyama T, Hashimoto T. 1999. Visualization of microtubules in living cells of transgenic *Arabidopsis*. *Protoplasma* 206, 201–206. [Google Scholar]
43. Wang YS, Motes CM, Mohamalawari DR, Blancaflor EB. 2004. Green fluorescent protein fusions to *Arabidopsis* fimbrin 1 for spatio-temporal imaging of F-actin dynamics in roots. *Cell Motility and the Cytoskeleton* 59, 79–93. [DOI] [PubMed] [Google Scholar]
44. Weise SE, Kiss JZ. 1999. Gravitropism of inflorescence stems in starch-deficient mutants of *Arabidopsis*. *International Journal of Plant Sciences* 160, 521–527. [DOI] [PubMed] [Google Scholar]
45. Weise SE, Kuznetsov OA, Hasenstein KH, Kiss JZ. 2000. Curvature in *Arabidopsis* inflorescence stems is limited to the region of amyloplast displacement. *Plant and Cell Physiology* 41, 702–709. [DOI]

[PubMed] [Google Scholar]

46. Wickner W. 2010. Membrane fusion: five lipids, four SNAREs, three chaperones, two nucleotides, and a Rab, all dancing in a ring on yeast vacuoles. *Annual Review of Cell and Developmental Biology* 26, 115–136. [DOI] [PubMed] [Google Scholar]
47. Yamamoto K, Kiss JZ. 2002. Disruption of the actin cytoskeleton results in the promotion of gravitropism in inflorescence stems and hypocotyls of Arabidopsis. *Plant Physiology* 128, 669–681. [DOI] [PMC free article] [PubMed] [Google Scholar]
48. Yamamoto K, Pyke KA, Kiss JZ. 2002. Reduced gravitropism in inflorescence stems and hypocotyls, but not roots, of Arabidopsis mutants with large plastids. *Physiologia Plantarum* 114, 627–636. [DOI] [PubMed] [Google Scholar]
49. Yamauchi Y, Fukaki H, Fujisawa H, Tasaka M. 1997. Mutations in the SGR4, SGR5 and SGR6 loci of *Arabidopsis thaliana* alter the shoot gravitropism. *Plant and Cell Physiology* 38, 530–535. [DOI] [PubMed] [Google Scholar]
50. Yano D, Sato M, Saito C, Sato MH, Morita MT, Tasaka M. 2003. A SNARE complex containing SGR3/AtVAM3 and ZIG/VTI11 in gravity-sensing cells is important for *Arabidopsis* shoot gravitropism. *Proceedings of the National Academy of Sciences of the United States of America* 100, 8589–8594. [DOI] [PMC free article] [PubMed] [Google Scholar]
51. Zheng J, Han SW, Munnik T, Rojas-Pierce M. 2014. *a* Multiple vacuoles in impaired tonoplast trafficking3 mutants are independent organelles. *Plant Signaling and Behavior* 9, e972113. [DOI] [PMC free article] [PubMed] [Google Scholar]
52. Zheng J, Han SW, Rodriguez-Welsh MF, Rojas-Pierce M. 2014. *b* Homotypic vacuole fusion requires VTI11 and is regulated by phosphoinositides. *Molecular Plant* 7, 1026–1040. [DOI] [PubMed] [Google Scholar]

Associated Data

This section collects any data citations, data availability statements, or supplementary materials included in this article.

Supplementary Materials

Supplementary Data

[supp_67_22_6459_index.html](#) (1.1KB, html)

[supp_ erw418_supplementary_figures_S1_S3.pdf](#) (1,011.3KB, pdf)

[Download video file](#) (9.6MB, avi)

[Download video file](#) (9.6MB, avi)

Articles from Journal of Experimental Botany are provided here courtesy of **Oxford University Press**